



**Australian
National
University**

**Intra-Tendinous Arterial Supply of the Gluteus Medius and
Minimus Muscles**

Mitchell John Raymond Kingston

u3954714

Date of Submission

July 2018

A thesis submitted for the degree of Master of Philosophy of The Australian National
University.

© Copyright by [Mitchell John Raymond Kingston] [2018]

All Rights Reserved

Statement of authorship of thesis.

I, Mitchell John Raymond Kingston, hereby declare that this submission is my own work and that it contains no material previously published or written by another person except where acknowledged in the text. Nor does it contain any material that has been accepted for the award of another degree or diploma in any university.

The thesis complies with the Australian National University requirements for a thesis as set out in https://policies.anu.edu.au/ppi/document/ANUP_012815.

Signature of Candidate: _____

Date: 15th July 2018

Supervisor Declaration

As supervisor of Mitchell John Raymond Kingston's Master of Philosophy, I certify that I consider this thesis entitled "Intra-Tendinous Arterial Supply of the Gluteus Medius and Minimus Muscles" to be suitable for examination

Signed: _____

Date: _____

Professor Paul N. Smith

Medical School

College of Health and Medicine

The Australian National University

Thesis Abstract

Gluteal tendinopathy is the most prevalent of all lower limb tendinopathies, and includes a spectrum of injury from inflammation to rupture/tear. The exact pathophysiology of tendinopathy is not understood with three theories currently being postulated. The vascular theory suggests that injury occurs at areas of hypovascularity within the tendon but a greater understanding of the intra-tendinous arterial supply of the gluteus medius and minimus muscles is important to examining the veracity of this theory.

The aim of this thesis was to describe and define the vascular supply of the gluteus medius and minimus tendons in the context of their macro- and micro-vasculature. A further aim was to examine the validity of using micro-computed tomography (CT) to visualise intra-tendinous arterial anatomy.

First, sixteen embalmed Wistar rats were used to investigate the accuracy of two contrast media (barium sulfate and lead oxide) to visualise and measure the extent of contrast penetration and diameter of blood vessels using micro-CT. There was no difference (mean difference [MD] 0.05; MD 95% confidence interval [CI] -0.83 to 0.93) between the number of branching generations for either filled vessels. The mean difference between the contrast medium and true cannula diameter was greater for lead oxide (0.11 mm) than barium sulfate (0.03 mm) when the cannulae were scanned at high resolution. Therefore, barium sulphate was used for the embalmed human cadaveric investigation.

Second, ten human cadaveric specimens were used to compare micro-CT angiography with three-dimensional (3-D) images and histological investigations (Haematoxylin and Eosin stain) of the intra-tendinous arterial supply of the gluteus medius and minimus muscle and

tendons. Prior to micro-CT all specimens were injected with contrast into blood vessels proximal to the tendon and scanned using CT. No intra-tendinous arteries were seen on the micro-CT images or histological slides. However, capillaries were visualised within the tendon enthesis, two mm from the tidemark, likely resulting from neovascularisation secondary to tendinopathic changes. These changes occurred at the common sites of gluteal tendon tears. The contrast filled to the ascending branch of the LCFA proximal to the greater trochanteric attachment of the gluteal tendons in only 30% of specimens; and in only 40% of the transverse branch. All LCFAs originated from the profunda femoris artery (PFA) compared to 50% of MCFAs. The remaining MCFAs arose from the femoral artery (40%) and a common trunk with the PFA (10%).

The modified Bonar scores, which quantified the extent of tendon degeneration ranged from 4 – 10 out of a possible 15 (worst). An incidental finding of muscle fat infiltrate was found distally in all specimens and proximally in only 50%.

These results suggest that micro-CT may not be a good method for assessing intra-tendinous arterial supply. However, penetration of the contrast may have been inhibited by using embalmed cadaveric specimens. There were no intra-tendinous vessels detected except for signs of neovascularisation secondary to tendon degeneration potentially supporting the vascular theory of tendon degeneration. Future studies would benefit from using fresh and younger specimens or *in vivo* techniques.

Acknowledgements

I would like to express my utmost gratitude to those people who made this thesis possible.

I owe my deepest gratitude to my supervisors.

To my Principal Supervisor, Professor Paul N. Smith for his ongoing support, guidance and opportunity to not only follow my surgical dreams but undertake this work concurrently.

To my Co-Supervisors, Dr. Diana M. Perriman and Dr. Alexandra L. Webb for their constant guidance, encouragement and unwavering optimistic support, without which this work would never have been possible.

To Dr. Jason Potas and his team, without whom the completion of the pilot contrast media study would not have been achieved.

To Dr. Mitali Fadia, without her guidance and expertise the histological portion of this work would not have been able to be completed.

To Dr. Michael Turner, Dr. Ajay Limaye and Dr. Levi Beeching, whose assistance using Drishti and performing the micro-CT scanning was invaluable.

To Mr. Adrian Meijer, Ms. Amy Krause and Ms. Mel Egan, whose assistance and performing the CT scanning was instrumental to the completion of this work.

To Dr. Teresa Newman, whose statistical expertise was utilised throughout this work.

To Ms Natalie Invten, whose artistic prowess have added depth to this body of work.

To Dr. Eric Thomas, whose motivation and inspiration helped me realise what I would need to sacrifice to achieve success.

To Mum, Dad and Nanna Iris, without you I would not be the person I am today.

Table of Contents

Statement of authorship of thesis.....	ii
Supervisor Declaration.....	iii
Thesis Abstract.....	iv
Acknowledgements.....	vi
Table of Contents	vii
List of Figures	xi
List of Tables	xiv
List of Appendices	xv
Publications and Presentations.....	xvi
Chapter 1: Introduction	15
1.1 Introduction	17
1.2 Pathophysiology of Tendinopathy.....	18
1.3 Tendon Arterial Anatomy	21
1.4 Gluteal Tendon Tears.....	23
1.5 Research Questions	26
Chapter 2: Literature Review	28
2.1. Gluteal Muscle Anatomy.....	30
2.1.1. Gluteus Medius.....	30
2.1.2. Gluteus Minimus.....	33

2.1.3. Conjoint Tendon	34
2.2. Gluteal Muscle Arterial Supply.....	35
2.3. Gluteal Arteries	35
2.3.1. Superior Gluteal Artery	35
2.3.2. Inferior Gluteal Artery	37
2.4. Circumflex Femoral Arteries	38
2.4.1. Lateral Circumflex Femoral Artery.....	39
2.4.2. Medial Circumflex Femoral Artery.....	42
2.5. Summary	46
Chapter 3: Contrast Comparison Study	48
Co-authors' Declaration.....	50
3.1. Introduction	51
3.2. Methods	54
3.2.1. Animals	54
3.2.2. Contrast Media Preparation	55
3.2.3. Micro-CT Scanning.....	56
3.2.4. Data Analysis.....	58
3.3. Results.....	59
3.3.1. General Aspects	59
3.3.2. Quantitative and Qualitative Measurements	60
3.3.3. Data analysis	61
3.4. Discussion.....	63
3.5. Conclusion	66

Chapter 4: Vascular Imaging Studies	68
4.1. Introduction	70
4.2. Methods	72
4.2.1. Exploratory Dissection Study	72
4.2.2. Cadaveric Specimens	72
4.2.3. Contrast Media Preparation	73
4.2.4. Specimen Preparation	73
4.2.5. Contrast Media Injection	74
4.2.6. CT Scanning.....	75
4.2.7. Dissection for Micro-CT	75
4.2.8. Micro-CT Scanning	77
4.3. Results.....	78
4.4 Discussion.....	83
 Chapter 5: Histological Study	 87
5.1. Introduction	89
5.2. Methods	92
5.2.1. Techniques for Matching Micro-CT to Histology	94
5.2.2. Histological Assessment.....	94
5.3. Results.....	98
5.3.1. Vessels	98
5.3.2. Tendon Degeneration	101
5.3.3. Muscle Degeneration.....	103
5.4. Discussion.....	106

Chapter 6: Conclusions 110

References..... 115

Appendix 1: Dissection Studies..... 133

List of Figures

Figure 1.1. Lateral view of the left hip showing the position of a gluteal tendon tear (from Bunker et al., 1997, with permission)	24
Figure 1.2. Lateral views of the right and left hip showing the Milwaukee Classification of gluteal tendon tears (from Davies et al., 2013 with permission)	25
Figure 2.1. Attachment sites of gluteus medius and minimus. Deep fascicular insertion (shaded area); gluteal aponeurosis insertion (hatching); tendinous attachments to greater trochanter (dots) (from Flack et al., 2014, with permission)	31
Figure 2.2. Branches of the lateral circumflex femoral artery	40
Figure 2.3. Varying nomenclature for the branches of the medial circumflex femoral artery. Modified from Clarke and Coburn (1993)	44
Figure 2.4. Branches of the medial circumflex femoral artery based on the descriptions by Gautier et al., 2000.....	46
Figure 3.1. Anterior view of three-dimensional reconstruction images of the embalmed rat lower limb vessels injected with barium sulfate resin (A) and lead oxide milk powder (B) contrast media	60
Figure 3.2. The mean difference (MD) and the variance of the estimates ($1.96SD = 1.96 \times \text{standard deviation of the differences}$) between the lead oxide milk powder (grey) and barium sulfate resin (black) and known internal cannulae diameter when micro-CT scanned at high (thick line) and low (thin line) resolution	62

Figure 4.1. Lateral view of Specimen 3, showing correlation of slide number to specimen prior to histological sectioning, using a similar grid pattern to that in Figure 5.2 76

Figure 4.2. 3-D micro-CT reconstruction of the right hip (Specimen 5), anterior view, showing the hip joint and circumflex vessels (A), and in relation to the gluteus medius and minimus muscles (B) 79

Figure 4.3. 3-D micro-CT reconstruction images showing the anterior view of the hip joint and contrast-filled vessels of Specimen 5 (left hip joint) showing incomplete filling of the terminal branches of IGA and AB of the LCFA (red circle) (A) and Specimen 8 (right hip joint), showing the filled terminal branches of AB of the LCFA and the decreased field of view that does not visualise the IGA (B) 81

Figure 4.4. Superior axial 3-D micro-CT reconstruction images showing two left hip joints and contrast-filled vessels in relation to the gluteal tendons. A. The contrast-filled vessels are coloured gold and there are none within the gluteal tendon (red circle). B. Some contrast-filled vessels are visible external to the gluteal tendons but not within the tendon..... 83

Figure 5.1. Cross-sectional representation of a tendon, showing the internal fascicles and tendon bundles and the outer layers (epitenon and paratenon) 90

Figure 5.2. Lateral view of right gluteal muscles of specimen 1. The marking sutures are overlaid with the grid pattern used to plan the histological section. In this figure the blue lines indicate the marking suture levels and the red squares indicate the location of the gluteal tendons 93

Figure 5.3. Proximal histological slide (slide 8, cross-sectional cut) of specimen 8 viewed at 20 x magnification 99

Figure 5.4. Neovascularisation of enthesis in histological section of specimen 11 (slide 15, cross-sectional cut), viewed at 10 x magnification 100

List of Tables

Table 3.1. Mean bias (95% CI) from low and high resolution micro-CT scan three-dimensional reconstructions, for cannulae of known ('true') internal diameter filled with barium sulfate resin or lead oxide milk powder	61
Table 3.2. Reliability of the internal diameter measurements of the contrast-filled cannulae three-dimensional reconstructions	62
Table 4.1. Micro-CT Scanning Parameters	77
Table 4.2 Origins of LCFA and MCFA as shown in the 3-D micro-CT reconstruction images	80
Table 4.3. Most distal point of contrast media filling of the Ascending Branch and Transverse Branch of the LCFA	82
Table 5.1. Bonar score adapted from Fearon et al. (2014)	96
Table 5.2. Position of vessels associated with the gluteal tendons	101
Table 5.3. Modified Bonar score for the most degenerative histological slide of each specimen	102
Table 5.4. Changes in muscle in proximal portion of specimen	104
Table 5.5. Changes in muscle in distal portion of specimen	105

List of Appendices

Appendix 1. Dissection studies..... 133

Publications and Presentations

Papers published/in press.

Kingston MJ, Perriman DM, Neeman T, Smith PN, Webb AL (2016) Contrast agent comparison for three-dimensional micro-CT angiography: A cadaveric study. *Contrast Media & Molecular Imaging* 11:319-324

Conference presentations.

Intra-Tendinous Arterial Supply of Gluteus Medius and Minimus, Australian Capital Territory Australian Orthopaedic Association Annual Scientific Meeting, 2017

Novel Technique for Visualising Intra-Tendinous Arterial Supply, Australian Capital Territory Australian Orthopaedic Association Annual Scientific Meeting, 2015

Systematic Review of Circumflex Femoral Arteries, Australian Orthopaedic Association Annual Scientific Meeting, 2014

Comparison of micro-CT 3D Angiography contrast agents, Australian Capital Territory Australian Orthopaedic Association Annual Scientific Meeting, 2014

Awards.

Best Student (Higher Degree) Presentation, Australian Capital Territory Australian Orthopaedic Association Annual Scientific Meeting, 2014

Chapter 1:

Introduction

Chapter 1: Introduction.

1.1 Introduction.....	17
1.2 Pathophysiology of Tendinopathy.....	18
1.3 Tendon Arterial Anatomy	21
1.4 Gluteal Tendon Tears.....	23
1.5 Research Questions	26

1.1 Introduction

Gluteal tendinopathy is the most prevalent of all lower limb tendinopathies (Albers et al., 2014). Tendinopathy is an umbrella term that indicates a non-rupture injury to a tendon or paratenon that can be exacerbated by mechanical loading (Scott et al., 2015). Tendinopathy includes tendinitis and tendinosis and both can result in tendon degeneration (Osti et al., 2017). Tendinopathy can occur in any tendon in the body, with the most commonly studied including supraspinatus, infraspinatus, patella, Achilles and long head of biceps brachii tendons (Brooks et al., 1992; Chen et al., 2009; Cheng et al., 2010). However, the gluteal tendons have attracted increased interest in recent years (El-Husseiny et al., 2011; Lachiewicz., 2011; Fearon et al., 2014).

Gluteal tendinopathy is most prevalent in women aged over 40 years with a peak incidence in the fourth to sixth decades of life. Patients suffering gluteal tendinopathy typically presents with an antalgic gait and disabling localized lateral hip pain that is worse with activities of daily living (such as sitting, climbing stairs and lying on the hip) (El-Husseiny et al., 2011). It is reported to affect up to 23.5% of women and 8.5% of men between the ages of 50 and 79 years with a female:male ratio of 4:1 (Connell et al., 2003; Lachiewicz, 2011; El-Husseiny et al., 2011; Grimaldi et al., 2015). Gluteal tendinopathy more commonly occurs unilaterally (Connell et al., 2003; Lachiewicz, 2011; Chandrasekaran et al., 2015).

The gluteal tendons have been reported to be involved in the majority of cases of Greater Trochanteric Pain Syndrome (GTPS) (Bird et al., 2001; Williams and Cohen, 2009; El-Husseiny et al., 2011; Davies et al., 2013; Reid, 2016). GTPS is described as lateral hip pain and pain on palpation over the lateral trochanter. It is thought to be more accurately

described as a regional pain syndrome that includes a myriad of etiologies (Williams and Cohen, 2009; Fearon et al., 2010; Fearon et al., 2014). People suffering from GTPS have significant disability and functional deficits, which are equivalent to patients with severe osteoarthritis (Fearon et al., 2014; Grimaldi et al., 2015). In an MRI study of 25 women with GTPS, 46% had gluteal tendon tears (Bird et al., 2001).

Gluteal tendinopathy is comprised of a spectrum from tendinosis through to low-grade partial and onto high-grade complete tears (Connell et al., 2003; Chi et al., 2015). The most common finding in a sonographic study of 75 people presenting with lateral hip pain was diffuse hypoechoic change within the gluteus medius tendon (Connell et al., 2013). A progression from tendinosis to tendon tear with increasing age has been observed (Chi et al., 2015). Gluteal tendon tears are thought to occur in degenerated tendons, which may or may not be symptomatic. Howell et al. (2001) reported a 20% prevalence of gluteal tendon tears at the time of total hip arthroplasty, whilst Bunker et al. (1997) found that 22% of patients undergoing operative management after neck of femur fractures also had gluteal tendon tears. This indicates that gluteal tendon tears may occur asymptotically and not be fully represented in the prevalence data.

1.2 Pathophysiology of Tendinopathy

There are two distinct types of tendon injuries, acute symptomatic tendinopathy from overuse or training errors, and chronic degenerative tendinopathic changes from an unknown etiology, which may or may not be symptomatic (Van Ginckel et al., 2009; El-Husseiny et al., 2011). This thesis will be focusing on chronic degenerative tendonopathy.

Tendinopathic tendons are thicker, but have reduced energy-storing capacity, meaning that for the same load they exhibit higher strains than healthy tendons (Scott et al., 2015).

Prominent features of chronic tendinopathic histopathology include: a disorganisation of collagen fibres; an increase in the number of vessels and sensory nerves; an increase in the hydrated components of the extracellular matrix; a breakdown of tissues (tendon/endotendon/paratenon) organisation; and haphazardly arranged proliferation of the smaller type III collagen fibres (Fu et al., 2010; Scott et al., 2015; Reid, 2016; Osti et al., 2017). The resulting accumulation of poor quality repair tissue in tendons is analogous to the healing after acute injury, except that with overuse tendinopathy, the injury-repair response evolves gradually over time (Scott et al., 2015).

The aetiology of tendinopathy is proposed to be multifactorial with both intrinsic and extrinsic factors but the exact mechanism remains unknown (Reid, 2016). There are currently three theories which address the pathophysiology of tendinopathy and these include: a mechanical theory; a metabolic theory; and a vascular theory (Chen et al., 2009; Gaida et al., 2009; Ranger et al., 2015; Scott et al., 2015; Tilley et al., 2015).

The mechanical theory suggests that tendons that are chronically exposed to excessive loading or cycles of injury and repair develop tendinopathy (Scott et al., 2015; Albers et al., 2016). The percentage of tenocytes that undergo apoptosis increased as the degree of damage to the extracellular matrix of the tendons increased (Wu et al., 2011). It is this increase in apoptotic cells that causes the histopathological changes of a tendinopathic tendon (Osti et al., 2017). Stress shielding and compression of the deep fibres of the gluteal tendons during hip adduction is thought to contribute in the development of tendon

degeneration (Grimaldi et al., 2015). However, this theory may not completely explain why non weight-bearing tendons become tendinopathic (Scott et al., 2015; Albers et al., 2016).

The metabolic theory suggests that there is a higher risk of tendinopathy in people with metabolic disorders or from medications (Gaida et al., 2009; de Olivera et al., 2013; Tilley et al., 2015). Gaida et al. (2009) observed that people suffering from obesity, diabetes mellitus or dyslipidaemias had a higher incidence of tendinopathy in both weight-bearing and non weight-bearing tendons compared to the general population. This observation was further investigated by Tilley et al. (2015) and Ranger et al. (2016) who found a link between dyslipidaemias and tendon structure as well as a threefold increase in the odds of tendinopathy in diabetic patients compared to controls. The molecular mechanism of the metabolic theory is not yet completely understood, but studies of degenerated tendons suggest that some enzymes may play a role in the tendon remodelling process (Sharma and Maffulli, 2005). In chronic Achilles tendinopathic specimens, a large down regulation in matrix metalloproteinase-3 (MMP-3) was observed (Ireland et al., 2001).

The third theory, the vascular theory, contends that tendinopathy is secondary to hypovascularity (Chen et al., 2009). Tenocytes are able to withstand reductions in blood perfusion and therefore hypoxia, however this may induce early tendinopathic changes via apoptotic pathways (Chen et al., 2009; Osti et al., 2017). Hypoxia-inducible factor 1 α (HIF-1 α) and Bcl-2 have been found at increased levels in biopsies from supraspinatus tendons with early tendinopathy changes (Millar et al., 2011). HIF-1 α is a critical regulator in the initiation of apoptosis and inflammatory processes (Miller et al., 2001). Hypoxia in tenocytes also reduces p38 production which increases type III collagen synthesis compared to type I, which decreases the resistance of tendons to tensile force (Millar et al.,

2011). The presence of these hypoxia-related proteins in early tendinopathy biopsies demonstrates that hypoxia from hypo-perfusion may play a role in regulating inflammatory and apoptotic mechanisms thus leading to shifts in the function and the repair cycle of tenocytes (Millar et al., 2011).

Degeneration and subsequent rupture of tendons has been associated with hypovascularity of specific regions within the Achilles and long head of biceps tendons (Fenwick et al., 2002; Chen et al., 2009; Cheng et al., 2010). Chen et al. (2009) investigated the Achilles tendon and found watershed zones in the midsection of the tendon, between the areas of perfusion from the posterior tibial and peroneal arteries, which is the area most frequently ruptured. Cheng et al. (2010) also showed that tendon tears most frequently occur in areas of poor to no arterial supply in the long head of biceps tendon.

1.3 Tendon Arterial Anatomy

Early investigators believed that tendons were avascular (Fenwick et al., 2002). During development, tendons have a rich blood supply but this diminishes as they mature and become less cellular (Peacock, 1958). This led to the belief that tendons were avascular in maturity (Peacock, 1958). However, evidence of cellular death and disintegration of collagen bundles in tendons has been observed with disruption of their blood supply (Peacock, 1958). It is therefore now accepted that, despite the presence of relatively few cells in mature tendons, tendons have a measureable metabolism and therefore require a vascular supply (Peacock, 1958; Cheng et al., 2010). Furthermore, it has been suggested that in some tendons, synovial diffusion may play a part (Gelberman, 1985). In any case, it is

acknowledged that there are more blood vessels associated with tendons than were previously thought (Fenwick et al., 2002). Although less vascular compared to other tissues, the location of ruptures in the most hypovascular areas within tendons, implicates the important role of the vascular supply in tendinopathy (Cheng et al., 2010).

The vascular supply of a tendon has been shown to arise from three distinct areas: the musculotendinous junction; the osteotendinous junction; and vessels from various surrounding connective tissues such as the paratenon, mesotenon and vincula (Peacock, 1958; Ahmed et al., 1998). Arterial vessels are generally arranged longitudinally within the tendon, passing around the collagen fibre bundles in the endotenon (Schatzker and Brånemark, 1969; Brooks et al., 1992).

There is a lack of agreement with respect to whether the vessels penetrate the osteotendinous junction to supply the tendon (Fenwick et al., 2002; Cheng et al., 2010). Schmidt-Rohlfing et al. (1992) state that vessels at the osteotendinous junction of the Achilles tendon do not pass directly from the bone into the tendon due to the presence of a cartilage layer between the tendon and bone. However, these vessels were observed to anastomose with those of the periosteum, forming an indirect link with the osseous circulation (Schatzker and Brånemark, 1969; Fenwick et al., 2002). This is in contrast to the findings of Cheng et al. (2010) in the long head of biceps tendon in which histological cross-sections showed arterial vessels crossing the osteotendinous junction to supply the tendon, with vascularisation of the tendon 1.2 – 1.5 cm from the tendon origin. This disagreement between authors may stem from the fact that they were observing different tendons.

Hypovascularity in tendons can occur in two ways (Peterson et al., 2000; Cheng et al., 2010). The first is the watershed mechanism. There are areas within a single tendon which lie between the supply of two different arteries where the tissues are nourished indirectly by diffusion. These are called watershed areas and are theoretically more vulnerable to injury and poor healing (Cheng et al., 2010). The second occurs in gliding tendons, in regions where the tendons run around a bony pulley (Petersen et al., 2000; Cheng et al., 2010). Formation of avascular fibrocartilage occurs due to compression of the tendons over the bone as they glide around a bony pulley (Petersen et al., 2000). The compression can be amplified by adjacent tendons (Petersen et al., 2000).

Identification of hypovascularity in tendons can be achieved by mapping arterial territories. By so doing, it is possible to identify whether hypovascularity is a contributing factor to the tendinopathic processes involved in tendon rupture and/or tendinopathy (Chen et al., 2009). Intra-tendinous arterial anatomy has been investigated in multiple ways including dissection, microdissection, histology, vascular injection studies (with India Ink, lead oxide, barium sulphate, latex), immunohistochemical and angiographic studies (Petersen et al., 2000; Chen et al., 2009; Cheng et al., 2010). Advances in imaging technology potentially offer more effective methods for visualising the 3-dimensional anatomy of the micro-vasculature of tendons.

1.4 Gluteal Tendon Tears

Tears involving the gluteus medius tendon may occur within the main body of the tendon or at its insertion and were found to most commonly occur at the intertrochanteric line of

the femur, affecting the anterior fibres in a transverse fashion (Howell et al., 2001; Connell et al., 2003; El-Husseiny, 2011). Tears of the mid and posterior fibres rarely occur (Connell et al., 2003). All tears are found within 1 cm of the anterior intertrochanteric line (Howell et al., 2001; Connell et al., 2003; El-Husseiny, 2011). The typical appearance of a gluteal tendon tear is that of a circular or oval defect in the conjoint tendon of gluteus medius and minimus at the osteotendinous junction at its insertion (Bunker et al., 1997). These tears usually have rolled, mature edges, and are often associated with the presence of free fluid in the trochanteric bursa and the bony surface of the greater trochanter is visible through the tendinous defect (Bunker et al., 1997).

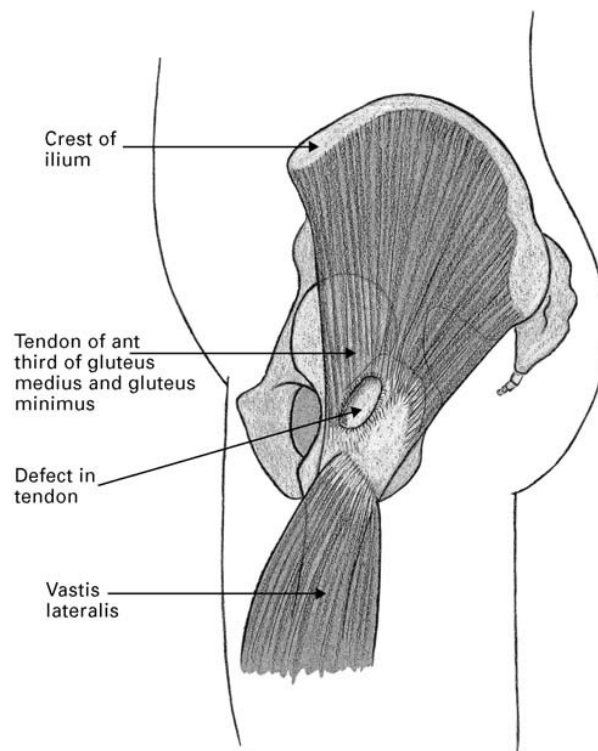


Figure 1.1. Lateral view of the left hip showing the position of a gluteal tendon tear (from Bunker et al., 1997, with permission)

Davies et al. (2013) devised a classification (the Milwaukee Classification) of gluteal tendon tears based on MRI and surgical findings, which is described on the hours of a clock face due to the differing tendon insertions between left and right hips as seen in Figure 1.2. Grade I is when one hour would be involved (for example 11 to 12 in Figure 1.2), Grade II is when two hours are involved, Grade III involves three hours and Grade IV is where there is nearly complete or complete detachment of the tendons (Davies et al., 2013).

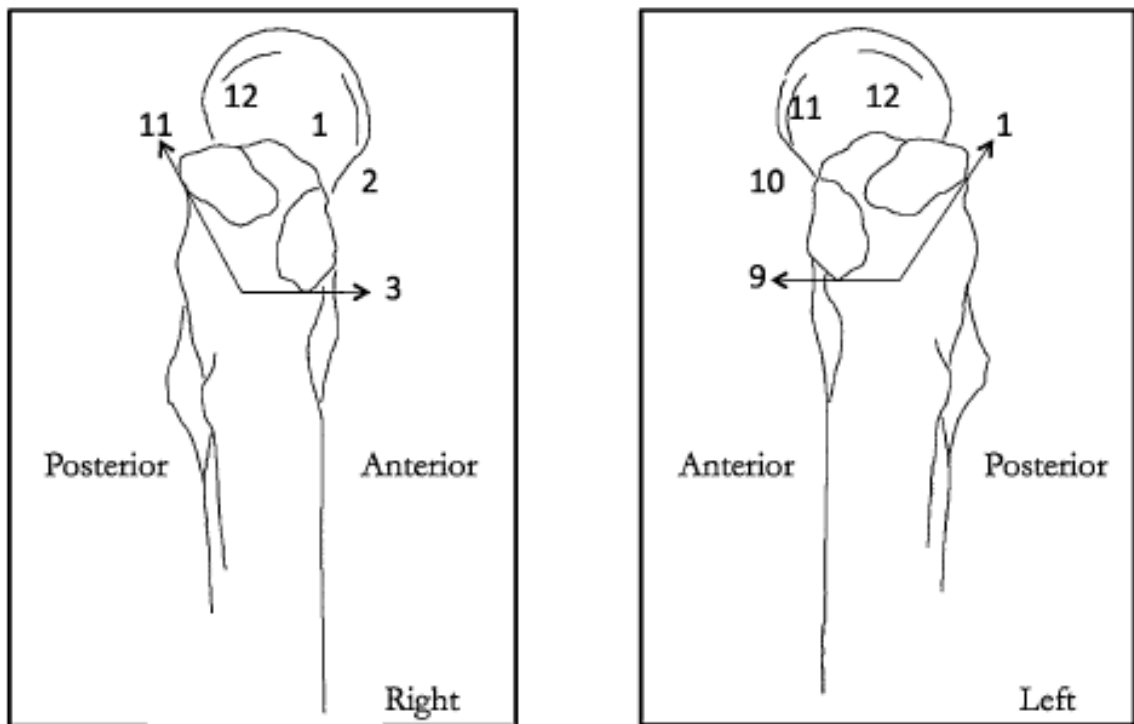


Figure 1.2. Lateral views of the right and left hip showing the Milwaukee Classification of gluteal tendon tears (from Davies et al., 2013 with permission)

The exact cause of gluteal tendon tears is unclear (Howell et al., 2001; El-Husseiny et al., 2011). Howell et al. (2001) suggested that most of the gluteal tears occur at the vascular watershed region, which lies within 1 cm of the intertrochanteric line (Figure 1) as has been described for both the long head of biceps and Achilles tendons (Chen et al., 2009; Cheng et al., 2010). However, the contention that a watershed area exists within the gluteal tendons has not yet been demonstrated. The underlying pathologic process is believed to be mediated by ischaemia with resultant degenerative changes at the osteotendinous junction leading to an eventual tear (Howell et al., 2001; Chen et al., 2009; Cheng et al., 2010).

Therefore, the overall aim of this thesis was to investigate the intra-tendinous arterial anatomy of the gluteal tendons and examine whether the vascular theory of tendinopathy applies to these tendons. More specifically, the aim was to describe and define the vascular supply of the gluteus medius and minimus tendons in the context of their macro- and micro-vasculature. In addition, the validity of using micro-Computed Tomography (micro-CT) to visualise intra-tendinous arterial anatomy was examined.

1.5 Research Questions

1. What is the arterial supply of the gluteal tendons?
2. Which of the known angiographic contrast media previously used in cadaveric studies most accurately represents vessel diameters from 3-D reconstructed micro-CT images?
3. Can micro-CT be used to accurately characterise intra-tendinous arterial anatomy?
4. Are there demonstrable areas of hypovascularity within the gluteal tendons?

5. Do areas of hypovascularity coincide with common sites of gluteal tears?
6. How degenerate are embalmed cadaveric tendons

Chapter 2:

Literature Review

Chapter 2: Literature Review.

2.1. Gluteal Muscle Anatomy.....	30
2.1.1. Gluteus Medius.....	30
2.1.2. Gluteus Minimus	33
2.1.3. Conjoint Tendon	34
2.2. Gluteal Muscle Arterial Supply.....	35
2.3. Gluteal Arteries	35
2.3.1. Superior Gluteal Artery	35
2.3.2. Inferior Gluteal Artery	37
2.4. Circumflex Femoral Arteries.....	38
2.4.1. Lateral Circumflex Femoral Artery.....	39
2.4.2. Medial Circumflex Femoral Artery	42
2.5. Summary	46

The purpose of this literature review is to describe the anatomy of gluteus medius and minimus as well as the morphology of their tendons and positions of the tendinous footprint. Given that this thesis is an exploration of the arterial supply of the gluteal tendons, the surrounding major arteries and their branches are described with respect to their origin and anatomical position. In addition, discrepancies of the nomenclature and previous anatomical descriptions are discussed.

2.1. Gluteal Muscle Anatomy

The gluteus medius and minimus muscles have been described as ‘the rotator cuff of the hip’ due to their anatomical similarity to the supraspinatus and infraspinatus muscles (Bunker et al., 1997; Flack et al., 2014).

2.1.1. Gluteus Medius

The gluteus medius has been reported to have three sites of proximal attachment as seen in Figure 2.1 (Flack et al., 2014). The first attachment for the deep fibres is to the gluteal fossa. Posteriorly, this attachment site extends from the posterior sacroiliac ligaments and along the length of the posterior gluteal line. Anteriorly, this attachment extends along the body of the ilium above the anterior gluteal line narrowing to a point at the anterior superior iliac spine (ASIS). The second attachment site from the deep surface of the gluteal aponeurosis was for the majority of the superficial fibres. Whilst the third attachment site

was from the posteroinferior edge of the iliac crest (El-Husseiny et al., 2011; Lachiewicz, 2011; Flack et al., 2014).

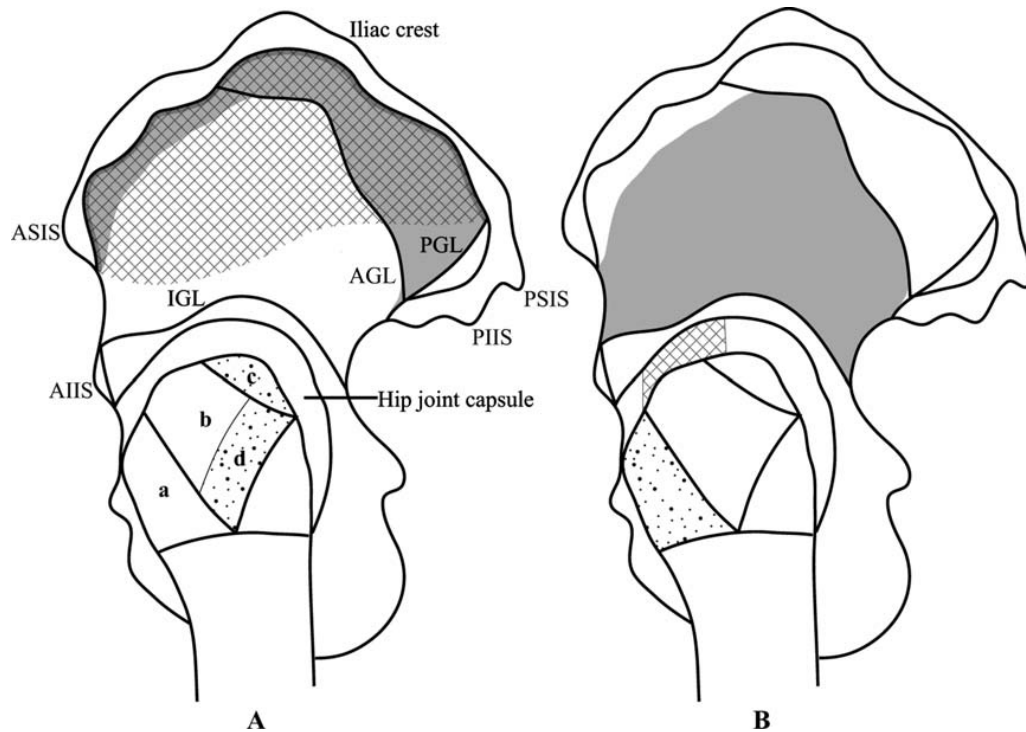


Figure 2.1. Attachment sites of gluteus medius and minimus. Deep fascicular insertion (shaded area); gluteal aponeurosis insertion (hatching); tendinous attachments to greater trochanter (dots). Abbreviations: A – gluteus medius; AGL – anterior gluteal line; AIIS – anterior inferior iliac spine; ASIS – anterior superior iliac spine; B – gluteus minimus; IGL – inferior gluteal line; PGL – posterior gluteal line; PIIS – posterior inferior iliac spine; PSIS – posterior superior iliac spine (from Flack et al., 2014, with permission)

There has been uncertainty as to whether the gluteus medius tendon is a singular tendon or is comprised of separate portions each with a different insertion sites (Duparc et al., 1997;

Standring et al., 2008; Pfirrmann et al., 2001). The method of investigation (cadaveric dissection versus magnetic resonance imaging) may have added to this uncertainty (Robertson et al., 2008; Pfirrmann et al., 2001). Recent cadaveric studies have shown that the gluteus medius tendon is composed of three distinctive parts (posterior, lateral, anterior), each with different attachment sites (Robertson et al., 2008).

The tendon has two insertions onto separate facets of the greater trochanter (GT) (Duparc et al. 1997; Robertson et al., 2008). The posterior part of the tendon inserts into the superoposterior facet of the GT, forming a cord-like attachment with a width stated as, 15.9 ± 3.2 mm (Flack et al., 2014) and 15.1 ± 3.1 mm (Tsutsumi et al., 2019). The lateral part of the tendon, inserts along an anteroinferior oblique line on the lateral facet of the GT after arising from the undersurface of the gluteus medius muscle (Hoffman and Pfirrmann, 2012; Flack et al., 2014). The mean width of this lateral attachment (30.8 ± 4.6 mm) has been reported to be significantly wider than the posterior attachment and longer in males than females (Flack et al., 2014). The anterior part is usually a muscular attachment onto the tendon of gluteus minimus (Hoffman and Pfirrmann, 2012).

Tsutsumi et al. (2019) described the gluteus medius tendon as containing a posterior and anterolateral parts, which correlate to the previous posterior and lateral descriptions (Robertson et al., 2008; Flack et al., 2014). The posterior portion of the tendon at its insertion is significantly thicker than the anterolateral portion (1.7 ± 0.4 mm vs 1.4 ± 0.4 mm, respectively) with the maximum thickness of the tendon showing the largest discrepancy in width (8.0 ± 1.8 mm vs 5.3 ± 1.2 mm, respectively) (Tsutsumi et al., 2019).

Gluteus Medius' primary function is to keep the pelvis parallel to the ground during the single-leg stance phase of gait by preventing the hip and contralateral limb from tilting inferiorly (Beck et al., 2000; Woyski et al., 2013). It has a secondary function is as a hip abductor and internal rotator (Woyski et al., 2013).

2.1.2. Gluteus Minimus

The proximal attachment of the gluteus minimus is to the external ilium as shown in Figure 2.1 (Flack et al., 2014). The line of attachment begins anteriorly 3 - 5 mm below the ASIS and runs posteriorly, parallel to the iliac crest, to the iliac tubercle. From this point, the attachment follows the anterior gluteal line to the greater sciatic notch, where the caudal portion of the muscle takes its origin from a tendinous sheet covering the hip joint capsule and the reflected head of rectus femoris (Beck et al., 2000; Flack et al., 2014). The posteroinferior border covers the posterosuperior acetabulum and follows the inferior gluteal line to the anterior inferior iliac spine. (Beck et al., 2000; Lachiewicz, 2011). The majority of fascicles arise from their attachment sites to form a flat, fan-shaped, aponeurotic tendon (Flack et al., 2014).

The tendon can be divided into two parts (lateral and medial) (Hoffman and Pfirrmann, 2012). The lateral part thickens distally before inserting into the lateral aspect of the anterior facet of the GT (Hoffman and Pfirrmann, 2012; Flack et al., 2014). The medial part is a deep tendinous slip that inserts into the superior hip joint capsule (Walters et al., 2001;

Hoffman and Pfirrmann, 2012; Flack et al., 2014). The aponeurotic tendon of gluteus minimus has been reported to measure 91.4 ± 10.4 mm in length and 56.8 ± 7.5 mm in width, with a distal attachment width of 21.5 ± 3.0 mm (Flack et al., 2014).

Gluteus minimus' primary function is to stabilise the head of the femur in the acetabulum, occurring mostly during extension of the hip (Beck et al., 2000). Gluteus minimus can act as a flexor and/or an abductor as well as either an internal or external rotator of the hip depending on which portion of the muscle is activated or the position of the femur relative to the acetabulum (Beck et al., 2000). The tendon of gluteus minimus helps to serve as a physical barrier against superolateral migration of the femoral head, therefore assisting with the primary function (Beck et al., 2000).

2.1.3. Conjoint Tendon

The distal tendons of gluteus medius and minimus fuse on approaching the anterior surface of the GT and become a conjoint tendon before inserting separately on the GT (Flack et al., 2014). The proximal end of this conjoint tendon begins at the level of the apex of the GT with a length of 19.8 ± 7.0 mm to its distal attachment. The distance from the proximal attachment of gluteus medius to the distal attachment of the conjoint tendon is 132.2 ± 23.2 mm (Flack et al., 2014).

2.2. Gluteal Muscle Arterial Supply

The gluteus medius and minimus muscles are supplied by the deep branch of the superior gluteal artery (SGA), which travels within the fascial plane between the two muscles (Ebraheim et al., 1998, Stecco et al., 2013). The ascending branch of the lateral circumflex femoral artery (LCFA) supplies muscular branches to the anterior aspect of gluteus medius and minimus (Vegas and Martin-Hervas, 2013; Wang et al., 2013).

2.3. Gluteal Arteries

The superior and inferior gluteal arteries are both branches from the internal iliac artery (IIA). The SGA is the largest branch of the IIA and is a continuation of its posterior division (Reddy et al., 2007). Whilst the inferior gluteal artery (IGA) is the larger of the terminal branches of the anterior division of the IIA (Reddy et al., 2007).

2.3.1. Superior Gluteal Artery

After branching from the IIA the SGA runs between either the lumbosacral trunk and the first sacral ventral ramus or between the first and second sacral ventral rami. The SGA leaves the pelvic cavity under the superior border of the greater sciatic foramen and above the piriformis muscle with the superior gluteal nerve (Song et al., 2006; Reddy et al., 2007; Bilhim et al., 2011).

The average distance from the origin of the SGA at the greater sciatic foramen to the posterior superior iliac spine has been found to measure 60 mm (Ebraheim et al., 1998) and 51 ± 9 mm (Song et al., 2006) in cadavers. From the posterior inferior iliac spine the origin of the SGA at the greater sciatic foramen has been reported to measure 42 mm (Ebraheim et al., 1998). The diameter of the SGA at the greater sciatic notch has been measured as 7 mm (range 6 – 9 mm) (Ebraheim et al., 1998).

After exiting through the greater sciatic foramen, the SGA gives off numerous muscular branches and then divides into superficial and deep branches (Reddy et al., 2007; Bilhim et al., 2011). The superficial branch of the SGA supplies the upper one third of the gluteus maximus muscle by entering its deep surface and has an average length of 21 mm (range 10 – 35 mm) (Ebraheim et al., 1998; Reddy et al., 2007).

The deep branch of the SGA travels within the fascial plane between the gluteus medius and minimus, where it divides into superior and inferior divisions. Before branching into its terminal branches, the deep branch of the SGA lies 6.3 ± 0.82 cm (anatomical dissection) and 5.2cm (CT angiography) from the GT, respectively (Stecco et al., 2013). The superior division runs along the superior border of gluteus minimus to the ASIS and anastomoses with the deep circumflex iliac artery of the external iliac artery (EIA) and the ascending branch of the LCFA (Ebraheim et al., 1998; Reddy et al., 2007).

The superior division of the deep SGA branch penetrates the gluteus medius an average of 29 mm from the ASIS, providing four to seven perforators to the gluteus medius and zero to two to the gluteus minimus (Ebraheim et al., 1998). The inferior division runs through the gluteus minimus, supplying both gluteus minimus and medius before anastomosing with the LCFA (Ebraheim et al., 1998; Reddy et al., 2007). The inferior division penetrates gluteus medius or minimus 36 mm from the ASIS, providing three to eight perforators to the medius and one to three to the minimus (Ebraheim et al., 1998).

2.3.2. Inferior Gluteal Artery

The IGA typically originates from the anterior division of the IIA. In rare cases it has been observed to originate from the internal pudendal or obturator arteries, and the absence of the IGA has been reported in one case (Yan et al., 2013). The IGA then passes posteriorly located anterior to the internal pudendal artery, and runs between the first and second or second and third ventral sacral rami (Reddy et al., 2007).

The IGA then leaves the pelvic cavity through the greater sciatic foramen below the piriformis muscle and medial to the sciatic nerve in 77.5% of cases (Gabrielli et al., 1997; Song et al., 2006; Bilhim et al., 2011). In the remaining cases, the IGA or one its branches perforates the sciatic nerve throughout its course (Gabrielli et al., 1997). The distance between the point at which the IGA traverses the greater sciatic foramen and the PSIS was reported to be 77 ± 10 mm (Song et al., 2006).

The IGA may also emerge as a common trunk with the SGA through the greater sciatic foramen at the superior margin of the piriformis where these arteries then separate and the IGA passes along the posterior aspect of the piriformis (Adachi, 1928). This occurrence was reported to have a frequency of between 0.2% - 4.4% in adults (Yan et al., 2013). In addition, Adachi (1928) also reported to have observed two or three cases in which the IGA passed through the piriformis muscle (Adachi, 1928).

The IGA continues to run inferiorly in the thigh as the descending branch between the greater trochanter and ischial tuberosity accompanying the sciatic and posterior femoral cutaneous nerves deep to the gluteus maximus (Windhofer et al., 2002). The IGA terminates by supplying the lower two-thirds of the gluteus maximus and the overlying skin as well as anastomosing with branches of the perforating arteries (Windhofer et al., 2002; Reddy et al., 2007; Bilhim et al., 2011). This descending branch was found in 108 of the 115 cadavers dissected by Windhofer et al. (2002).

2.4. Circumflex Femoral Arteries

The circumflex femoral arteries are considered the most important collateral branches of the profunda femoris artery (PFA), however, other variations of their origins have also been described (Vazquez et al., 2007). The lateral and medial circumflex femoral arteries are important because they play a significant role in the blood supply to the hip joint and surrounding structures as well as being at risk of injury during distal extension of the

Smith-Petersen approach¹ (Clarke and Colburn, 1993; Dixit, 2011; Anwer et al., 2014; Havalder et al., 2014; Grob et al., 2015). Their significance to the gluteal tendons is uncertain at present. It is postulated that the deep branch of the medial circumflex femoral artery (MCFA) may be significant for the blood supply to the gluteal tendons due to its proximity to the gluteal tendon insertion footprint on the greater trochanter on its path to supplying blood to the femoral head (Gauiter et al., 2000).

2.4.1. Lateral Circumflex Femoral Artery

The LCFA has been found to arise from the PFA in 70 - 83% of cases (Lipshutz, 1916; Adachi, 1928; Xu, 1989; Heitmann et al., 1998; Dixit et al., 2001; Vazquez et al., 2008; Uzel et al., 2008; Tansatit et al., 2008; Prakash et al., 2010; Dixit et al., 2011; Kalhor et al., 2012; Sinkeet et al., 2012; Anwer et al., 2013; Peera and Sugavasi, 2013; Anjankar et al., 2014; Manjappa and Prasanna, 2014; Nasr et al., 2014). The most common variant is when the LCFA originates from the femoral artery (FA). This occurs in 15 - 22% of cases (Siddarth et al., 1985; Xu et al., 1989; Tai et al., 2005; Vazquez et al., 2008; Uzel et al., 2008; Prakash et al., 2010; Anwer et al., 2013; Peera and Sugavasi, 2013; Anjankar et al., 2014; Manjappa et al., 2014; Nasr et al., 2014).

From its origin, the LCFA courses laterally through the femoral triangle and passes either between the superficial and deep branches of the femoral nerve, or deep to the femoral

¹ Anterior approach to the hip joint also known as the anterior iliofemoral approach, first described by Marius N. Smith-Petersen in 1917 (Patnaik et al, 2001; Rachbauer et al, 2009). This is the only surgical approach to the hip, which avoids muscle splitting and has been used for hip irrigation, surgical dislocation and more recently, hip arthroplasty (Patel and Stover, 2015).

nerve (Chummy, 2006; Orebaugh et al., 2006; Uzel et al., 2006; Anwer et al., 2013). The LCFA then leaves the femoral triangle beneath the sartorius muscle to lie deep to the rectus femoris muscle where it divides into three branches: ascending branch (AB); transverse branch (TB); and descending branch (DB) as shown in Figure 2.2 (Siddarth et al., 1985; Xu et al., 1989; Valdatta et al., 2001; Chummy, 2006; Choi et al., 2007; Stranding, 2008; Tansatit et al., 2008; Uzel et al., 2008; Tayfur et al., 2010; Wang et al., 2012; Vegas and Martin-Hervas, 2013). An oblique branch (OB) of the LCFA, with a variable origin, has also been described in 35% of 89 anterolateral thigh flaps (Wong et al. 2009).

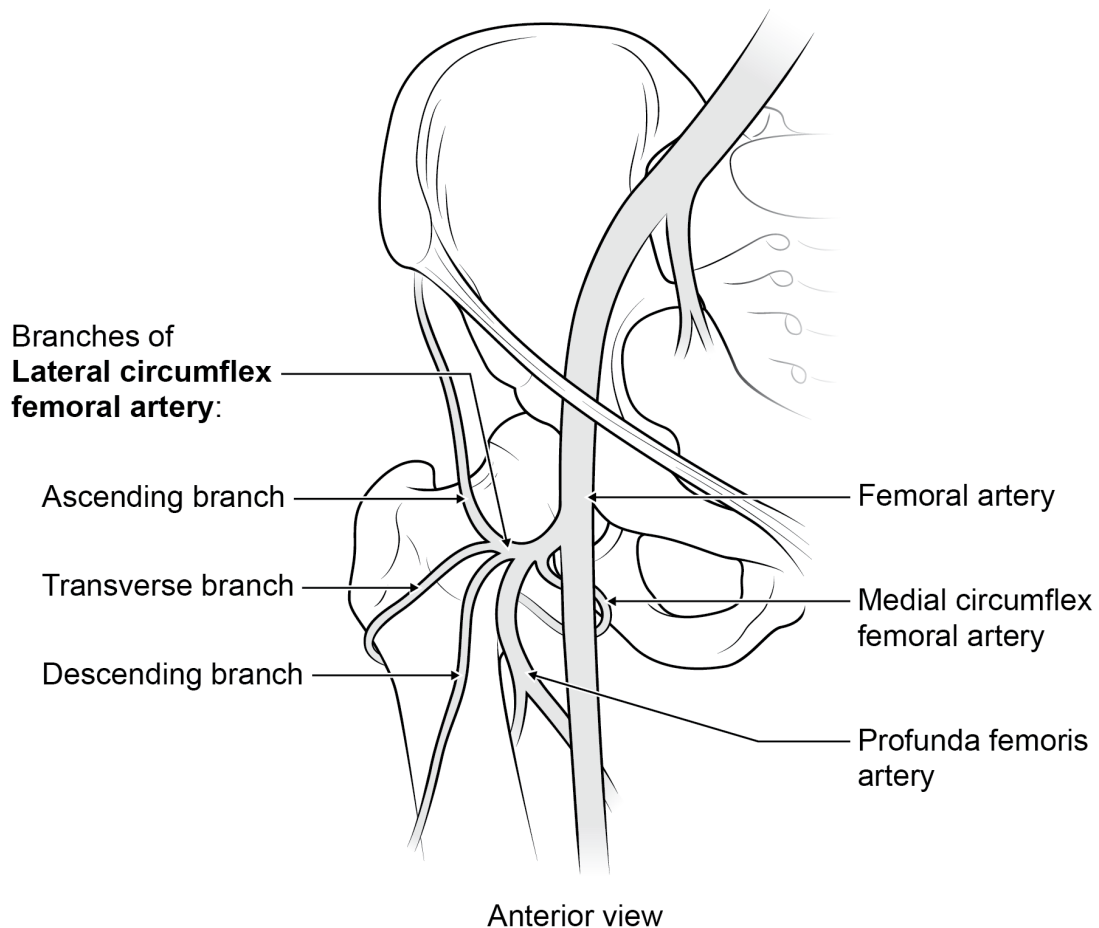


Figure 2.2. Branches of the lateral circumflex femoral artery

After branching from the LCFA, the TB runs laterally below the sartorius and rectus femoris muscles to supply the tensor fascia latae (Heitmann et al., 1998; Chummy, 2006; Stranding, 2008; Kalhor et al., 2012). Deep to the iliopsoas and rectus femoris, the TB gives off a capsular branch that supplies the anterior capsule of the hip joint and the overlying iliopsoas and rectus femoris (Kalhor et al., 2012). The origin of the TB is reported to be a mean of 24 mm (18 – 31 mm) from the origin of the LCFA (Wang et al., 2013). Given the capsular branch to the anterior capsule of the hip from the TB, and its proximity to the gluteal tendons, the significance of this vessel with regards to the blood supply of the gluteal tendons is uncertain.

The AB passes posteriorly to the divisions of the femoral nerve, on vastus lateralis beneath the sartorius and rectus femoris muscles, and gives branches to rectus femoris, vastus lateralis (proximal part), the hip joint and proximal femur (Chummy, 2006). Before entering the tensor fascia latae, the AB has been observed to give off one or more branches, which supply the anterior aspect of gluteus medius and minimus (Vegas and Martin-Hervas, 2013). Two terminating branches of the AB have been described. The trochanteric branch courses laterally over vastus intermedius and then deep to vastus lateralis and ends by dividing into two branches, which enter the inferior part of the greater trochanter (Howe et al., 1950; Bradnock, 1991). The gluteus medius branch arises from the AB and courses upwards laterally to the side of the tensor fasciae latae (Wang et al., 2013).

From its origin, the DB descends posterior to rectus femoris, giving off a muscular branch to the proximal third of this muscle, before continuing along the anterior border of vastus lateralis (Chummy, 2006; Standring et al., 2008; Tansatit et al., 2008; Wang et al., 2013). The DB is accompanied by two veins and laterally by the nerve to vastus lateralis as it courses towards the vastus lateralis. It then travels within the intermuscular septum between the rectus femoris and vastus lateralis to the knee where it anastomoses with the lateral superior genicular branch of the popliteal artery (Chummy, 2006; Standring et al., 2008; Valdatta et al., 2002; Tansatit et al., 2008).

When the OB is present, its course is between the TB and DB (Wong and Wei, 2009). The OB is visible lateral to the DB in the proximal thigh within the fascia between rectus femoris and vastus lateralis. Distally, it pierces and supplies the proximal third of vastus lateralis (Wong and Wei, 2009).

2.4.2. Medial Circumflex Femoral Artery

The medial circumflex femoral artery (MCFA) has been found to arise from the PFA in 60 - 83% of cases (Lipshutz, 1919; Adachi, 1928; Siddarth et al., 1985; Dixit et al., 2001; Basar et al., 2002; Tanyeli et al., 2006; Vazquez et al., 2007; Çiftcioglu et al., 2009; Prakash et al., 2010; Dixit et al., 2011; Zlotorowicz, et al., 2011; Kalhor et al., 2012; Anwer et al., 2013; Lalovic et al., 2013; Nasr et al., 2013; Shiny Vinila et al., 2013; Peera and Sugavasi, 2013; Havalader et al., 2014; Manjappa and Prasanna, 2014; Al-Talawah, 2015). The most common variant is when the MCFA originates from the FA. This occurs in 6.4 -

40% of cases (Lipshutz, 1919; Adachi, 1928; Clarke and Colburn, 1993; Dixit et al., 2001; Anwer et al., 2013; Kalhor et al., 2012; Gautier et al., 2000; Tanyeli et al., 2006; Lalovic et al., 2013; Prakash et al., 2010; Zlotorowicz, 2011). Absence of the MCFA is a rare occurrence with an incidence of 0.3 – 4.8% (Lipshutz, 1916; Adachi, 1928; Lalovic et al., 2012).

From its origin, the MCFA usually passes between the iliopsoas and pectineus muscles (Adachi, 1928; Howe et al., 1950; Kasai et al., 1985; Kalhor et al., 2012). A variant course has been observed in 6 – 13% of cases where it travels between the pectineus and adductor longus muscles (Adachi, 1928; Kasai et al., 1985).

The number of branches which arise from the MCFA is unclear. The literature is divided in terms of how many branches are identified and their nomenclature (Kasai et al., 1985; Clarke and Colburn, 1993; Chummy, 2006; Standring et al., 2008; Gautier et al., 2000; Zlotorowicz et al., 2011). Up to eight branches have been identified, however, the most recent report describes only five (Gautier et al., 2000). The discrepancies in these descriptions are summarised in Figure 2.3.

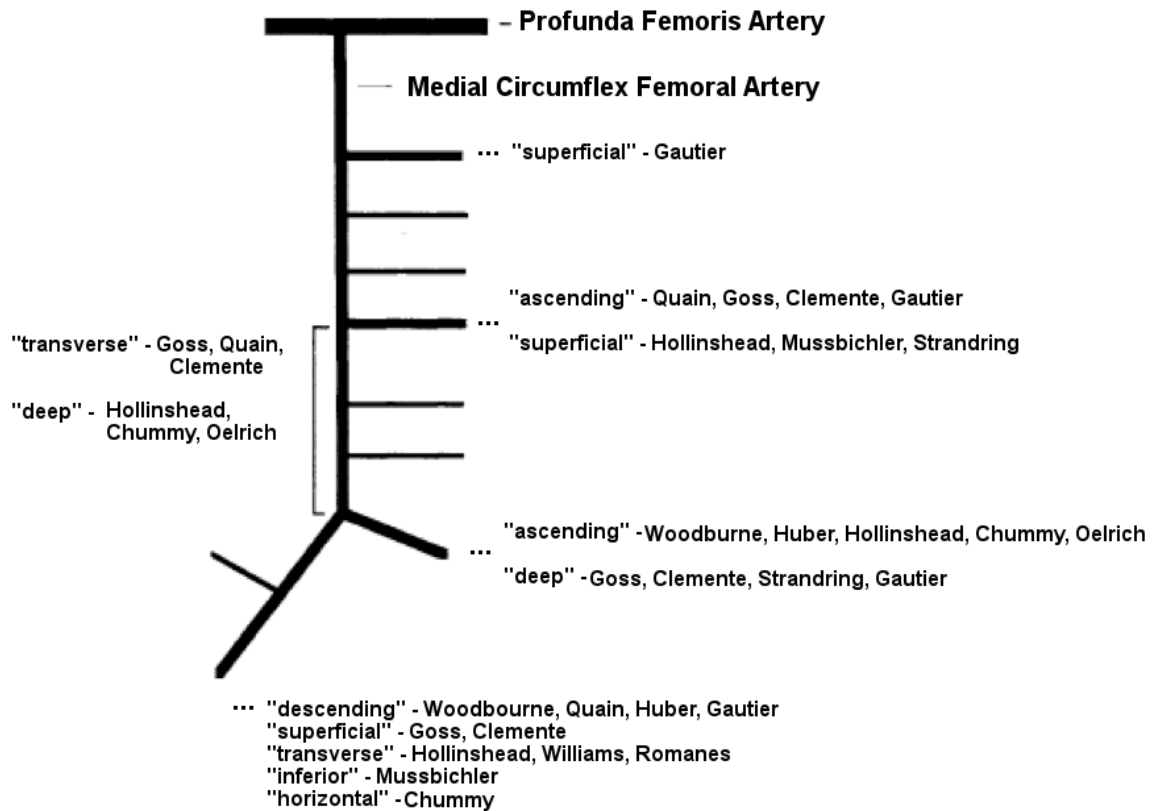


Figure 2.3. Varying nomenclature for the branches of the medial circumflex femoral artery. Modified from Clarke and Coburn (1993).

For clarity, the branches of the MCFA will be described using the five “consistent” branches outlined by Gautier et al. (2000) and shown in Figure 2.4:

- (i) Superficial branch - the first branch which courses between pectineus and adductor longus.
- (ii) Ascending branch - the next branch that arises and supplies the adductor brevis, adductor magnus and obturator externus muscles;

- (iii) Acetabular branch - observed in up to 37% of individuals. If present, it is described as ascending along the medial border of the iliopsoas and entering the hip joint through the acetabular notch (Kasai, 1985);
- (iv) Descending branch - a terminal branch of the MCFA that courses between the quadratus femoris and adductor magnus muscles ultimately supplying the ischiocrural muscles (Gautier et al., 2000).
- (v) Deep branch - the second terminal branch. It runs posterior to the obturator externus muscle and anterior to the quadratus femoris, it then crosses the anterior aspect of the superior gemellus, obturator internus and inferior gemellus tendons and enters the hip joint capsule to supply the head of the femur (Gautier et al., 2000; Zlotowicz et al., 2011)

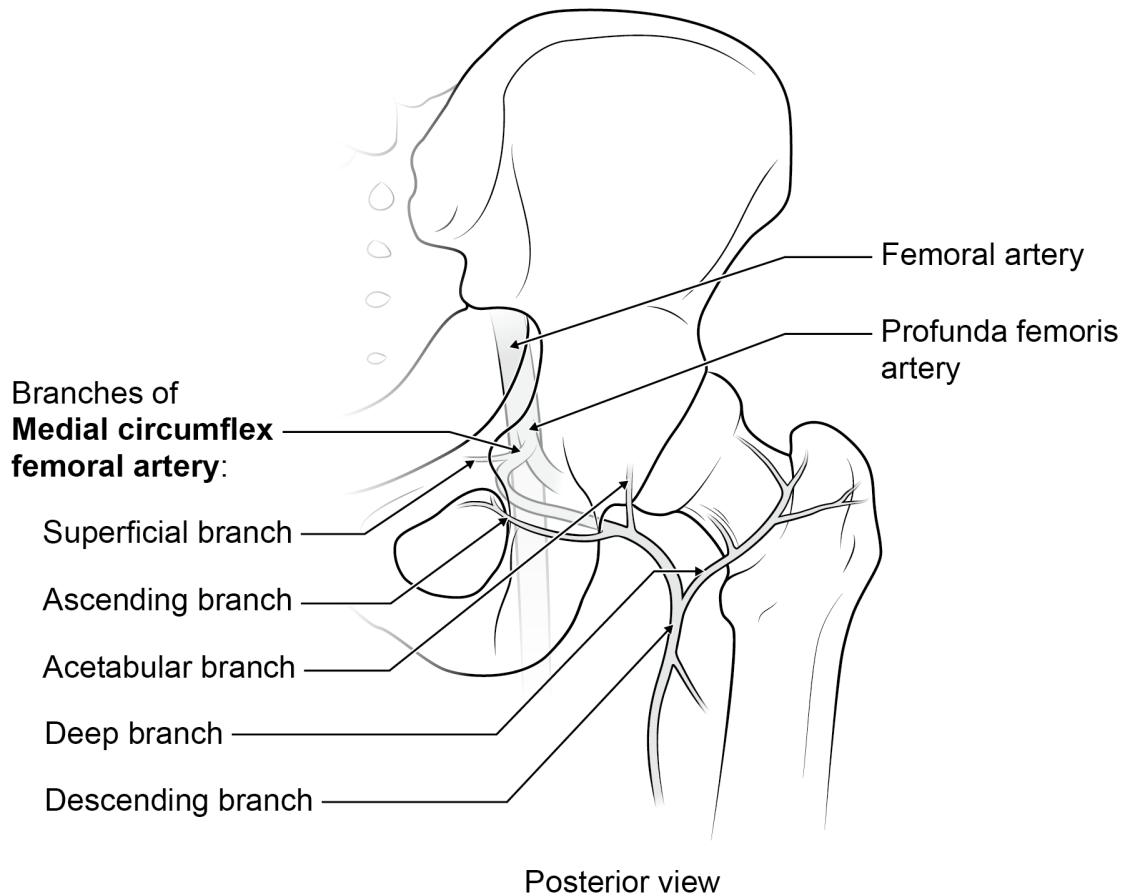


Figure 2.4. Branches of the medial circumflex femoral artery based on the descriptions by Gautier et al., 2000

2.5. Summary

In summary, the major focus of this thesis is an assessment of the intra-tendinous arterial supply of the gluteus medius and minimus. Due to their proximity to the gluteal tendons and their insertion into the greater trochanter, the deep branch of the MCFA and the TB of the LCFA are of most interest. The gluteus medius and minimus musculature is supplied by branches of the SGA, and the AB of the LCFA. The significance of these vessels with

regards to the arterial supply of the tendons is uncertain and of significant interest within this thesis.

Chapter 3:

Contrast Comparison Study

This chapter has been published in Contrast Media and Molecular Imaging:

Kingston MJ, Perriman DM, Neeman T, Smith PN, Webb AL (2016) Contrast agent comparison for three-dimensional micro-CT angiography: A cadaveric study. Contrast Media & Molecular Imaging 11:319-324

Chapter 3: Contrast Comparison Study.

Co-authors' Declaration.....	50
3.1. Introduction.....	51
3.2. Methods	54
3.2.1. Animals.....	54
3.2.2. Contrast Media Preparation.....	55
3.2.3. Micro-CT Scanning	56
3.2.4. Data Analysis	58
3.3. Results.....	59
3.3.1. General Aspects.....	59
3.3.2. Quantitative and Qualitative Measurements	60
3.3.3. Data analysis.....	61
3.4. Discussion.....	63
3.5. Conclusion	66

Co-authors' Declaration.

As co-authors of the paper "**Contrast agent comparison for three-dimensional micro-CT angiography: A cadaveric study**", we confirm that Diana Perriman and Alexandra Webb have made the following contributions:

- Conception and design of the research proposal,
- Analysis and interpretation of the findings,
- Writing the paper and critical appraisal of content, and
- Corresponding author for journal communication and publication peer-review process.

Co-author name Diana Perriman

Signed: _____

Date: _____

Co-author name Alexandra Webb

Signed: _____

Date: _____

CT angiography: A cadaveric study", we confirm that Teresa Neeman has made the following contributions:

- Analysis and interpretation of the findings

Co-author name Teresa Neeman

Signed: _____

Date: _____

3.1. Introduction

A thorough and accurate knowledge of microvascular networks in the human body is necessitated by continued advances in reconstructive surgical procedures such as perforator and osteomyocutaneous flaps (Brantner et al., 2015; Rath et al., 1990; Tregakiss et al., 2007). This has led to renewed interest in advanced imaging techniques that enable comprehensive visualisation of microvascular networks in cadavers which can be used to inform surgical applications (Rath et al., 1990; Tregakiss et al., 2007; Bulla et al., 2014; Rees and Taylor, 1986). Early anatomists used x-ray angiography to visualise and describe microvasculature morphology. This traditional technique has been considerably improved by recent advances in computerised tomography (CT) and micro-CT (micro-CT) technology. However there is a lack of clarity concerning which contrast medium is optimal to characterise vascular branching geometry and measure vessel dimensions accurately.

X-ray angiography overcame the disadvantage of tissue destruction associated with corrosion casting and dissection techniques to study blood vessels injected with latex, silicone or India ink (Bulla et al., 2014). However, the two-dimensional (2D) x-ray images generated did not enable distinction between vessels in different tissue layers or the identification of vessels coursing through different tissue planes (Tregakiss et al., 2007). The advent of CT angiography has created a non-destructive technique for three-dimensional (3D) visualisation of microvascular networks (Tregakiss et al., 2007, Bulla et al., 2014; Pauwels et al., 2013).

However, the accuracy of 3D reconstruction models generated from CT angiograms is limited due to the slice thickness being greater than the size of the microscopic vessels (Chen et al., 2011). To overcome these limitations, Ghanavati et al. (2014) utilised micro-CT angiography to obtain high-resolution 3D images of the mouse cerebral microvasculature. The radiopaque contrast agents used for micro-CT angiography need to be low viscosity and contain atoms with a high atomic number to enable the contrast-filled microvasculature to be differentiated from surrounding soft tissue structures (Pauwels et al., 2013; Ghanavati et al., 2014). Barium sulfate- and lead oxide-based contrast media are the most popular with lead oxide described as the 'gold standard' for visualisation of the finest microvascular networks (Bergeron et al., 2006).

Lead oxide mixed with gelatine is an inexpensive, simple and reliable method that results in very dense radiopacity (Bergeron et al., 2006). Milk powder has been substituted for gelatine in the x-ray angiography of embalmed cadavers with results equal to those achieved with the lead oxide and gelatine preparation injected into fresh cadaveric specimens (Rees and Taylor, 1986; Pan et al., 2010). Lead oxide, however, is toxic (Bergeron et al., 2006; Quinodoz et al. 2002). Stringent personal protective equipment (PPE) protocols are required for the use of lead oxide and any residues and contaminated equipment require specialist disposal (Bergeron et al., 2006). Barium sulfate, in contrast, is non-toxic. Typically mixed with gelatine or latex to achieve a thin consistency for optimal dispersal into the fine vessels, a new technique mixing barium sulfate with epoxy resin has recently been reported for CT angiography (Bulla et al., 2014; Bergeron et al., 2006). There

was agreement, to the smallest detectable arteries (0.1 mm diameter), between the CT angiographic images and corresponding dissection studies (Bulla et al., 2014).

No studies to date have directly compared lead oxide and barium sulfate based preparations to characterise vascular branching geometry and accurately measure vessel dimensions using micro-CT in embalmed specimens. Although lead oxide is widely used, it is highly toxic and therefore sub-optimal in terms of safety. If barium sulfate preparations can produce equally detailed images then it is arguably a better contrast medium. We hypothesised that barium sulfate can produce micro-CT 3D angiographic images that are equivalent in detail and accuracy to those produced by a lead oxide preparation.

Thus, the aim of this study was to establish whether barium sulfate combined with resin or gelatine is an equally effective contrast medium compared to a lead oxide-milk preparation when used with micro-CT 3D angiographic images in embalmed rodents. The specific questions addressed include:

1. Is barium sulfate resin (BS-R) and/or barium sulfate gelatine (BS-G) equivalent to lead oxide-milk powder (LO-M) in terms of the extent to which it perfuses into the lower limb vessels for the characterisation of vascular branching geometry in a rat model?
2. Which of the contrast media most accurately represents a known diameter when measurements are made from 3-D reconstructed micro-CT images?

3.2. Methods

3.2.1. Animals

Sixteen rats (male Wistar; 8 weeks of age) were perfused with a solution of 4% formaldehyde in phosphate buffered saline solution, following lethal barbitone injection, to enable fixation of the intact circulatory system whilst maintaining the patency of the blood vessels. These animals were obtained from another experiment and had undergone electrophysiological investigations of the sciatic nerve. Dissection of the anterior thorax and mediastinum of the rats was then undertaken to facilitate the insertion of a 20 G cannula (Introcan Safety, Braun, Melsungen, Germany) which was placed and secured into the thoracic aorta with 2-0 vicryl surgical ties (Ethicon Inc, Somerville, United States), after the arch of the aorta was ligated proximal to the cannula insertion site. The study was approved by the Australian National University Animal Experimentation Ethics Committee (A2014/36) and was conducted in accordance with the National Health and Medical Research Council's Australian Code of Practice for the Care and Use of Animals for Scientific Purposes and the ACT Animal Welfare Act (1992).

The toes of the left foot of each rat were transected for visual inspection of when the contrast preparation had extended distally to the end of the limb. Ten millilitres (ml) of 6% hydrogen peroxide solution (Orion Laboratories Pty. Ltd., Balcatta, Australia) was injected into the cannula and left in the vessels for 1-2 hours. Oxygen bubbles from the hydrogen peroxide distend the vessels (Ghanavati et al., 2014; Suami et al., 2007). The visible vessels

were inspected for hydrogen peroxide leakage. Identified leaks were secured with 2-0 vicryl surgical ties and/or quick-drying super glue.

3.2.2. Contrast Media Preparation

The three contrast agents were prepared and injected as follows:

3.2.2.1. Barium Sulfate Resin (BS-R) Preparation

Fifty grams of barium sulfate (E-Z-HD™, E-Z-EM, Westbury, United States) was thoroughly combined with 80 ml of compound A (Kinetix® R118 Infusion Resin, ATL Composites, Molendinar, Australia) and 20 ml of compound B (Kinetix® H120 Infusion Hardener, ATL Composites, Molendinar, Australia) in a fumehood. The solution was then degassed in the fumehood prior to injection (Bulla et al., 2014).

3.2.2.2. Barium Sulfate Gelatin (BS-G) Preparation

One hundred ml of Milli-Q water was heated to 40°C before 3 g of gelatine powder (Johnson & Johnson Pacific, Ultimo, Australia) and 5 ml of Listerine® (Johnson & Johnson Pacific, Ultimo, Sydney) was gradually added to the water and stirred continuously until the gelatine was dissolved. Fifty grams of barium sulfate (E-Z-HD™, E-Z-EM, Westbury, United States) was then added while the mixture was continuously stirred until an emulsion was formed (Chan et al., 2010). This formulation was modified from the preparation described by Chan et al. (2010) who used 40 g of barium sulphate in 100 ml of normal saline and 3 g of gelatine. The modification allowed for the concentration of barium sulfate to be equal in the BS-R and BS-G preparations.

3.2.2.3. Lead Oxide Milk (LO-M) Powder Preparation

One hundred grams of lead oxide (Pb_3O_4 red lead; Ajax Chemicals, Australia), 18 g of baby milk powder (Johnson & Johnson Pacific, Ultimo, Sydney) and 20 ml of tap water were mixed using a pestle and mortar and ground into a smooth paste. Boiling water (40 ml) was added to the paste and thoroughly stirred and combined (Pan et al., 2010).

Each contrast agent was independently injected into the aorta of 16 rats (six BS-R; five BS-G; five LO-M) using a 50 ml syringe in a pulsatile fashion to avoid supra-physiological pressures (Pan et al., 2010; Suami et al., 2007). The injections were conducted inside a fumehood. Appropriate personal protective equipment was used based on the relevant material safety data sheets and risk assessments. Perfusion was judged to be adequate when the contrast agent was observed to leak from the transected toes of the left foot.

Polymerisation of both the BS-R and BS-G preparations and solidification of the LO-M preparation was checked by assessing the residuals. In addition, four cannulae of known diameter (ranging from 18 G to 24 G in size [1.3, 1.1, 0.9, and 0.7 mm internal diameter]) were injected with each contrast agent. The rats and cannulae were labelled and placed in a coolroom at 4°C and left for 48 hours.

3.2.3. Micro-CT Scanning

The injected rats and cannulae were scanned using a Quantum FX Micro-CT scanner (PerkinElmer, Waltham, Massachusetts). The rats were positioned prone head first in the

scanner. Two sets of cannulae were scanned simultaneously to directly compare the contrast media. The cannulae were arranged so that the smallest cannula containing each contrast medium was positioned directly opposite each other. Two sequence parameters were used to produce: a low resolution/large scan area (field of view (FOV) = 70; voxel size = 295 μm ; 90 kV; 200 μA); and a high resolution/small scan area (FOV = 30; voxel size = 59 μm ; 90 kV; 200 μA).

3.2.3.1 Three-dimensional reconstructions

Three-dimensional reconstructions of the contrast-filled blood vessels and cannulae were created using the 3D volume rendering tool in Osirix MD (Pixmeo, Geneva, Switzerland). The 3D reconstructions of the blood vessels were then analysed. The number of branching generations of the vessels was counted in both the right and left lower limb of each rat.

3.2.3.2 Quantitative measures

The first branching generation was the bifurcation of the aorta and each continuous branching artery from this point was allocated a generation number. The greatest number of branching generations for each limb was recorded.

The diameter of the smallest visible vessel was then measured. Each 3D reconstruction of the rat lower limb vessels was divided into eight sections. The smallest vessel in each section was measured using the Osirix MD measurement tool. The diameter of the smallest vessel, out of the eight sections, was recorded for each rat.

Ten measurements were taken along the length of the 3D reconstruction of each cannula to quantify the internal diameter, using the Osirix MD measurement tool. The average of the ten measurements was calculated.

3.2.4. Data Analysis

Question one was examined in two ways. First, the extent of perfusion was examined by counting the maximum number of branching generations as above. These were compared between contrast media using ANOVA adjusting for side (left/right). Predicted means, mean differences, standard errors of the means and 95% confidence intervals of the mean difference (MD 95% CI) were reported. Second, the smallest visible vessel diameter was measured and compared using the same analysis.

Question two was examined by comparing the bias and variance of the estimates relative to the known cannula diameter (Bland and Altman, 1999). Differences in the internal diameter between the known cannula diameter supplied by the manufacturer, and the measurements of the contrast-filled cannulae scanned at both low and high resolutions (bias), were graphed against the known diameter. In addition, differences in bias between the two contrast media were analysed using ANOVA controlling for resolution (low/high). The results of the ANOVA were reported as marginal means and standard errors for each contrast medium and the difference between the marginal means (MD) and 95% confidence intervals of the difference (MD 95% CI). Intra-observer reliability (measurements made two weeks apart by the same observer) and inter-observer reliability (measurements made

by a second observer trained and blinded to the results of the first observer) were examined for all cannulae measurements using intra-class correlation coefficients (ICCs). All analyses were performed using SPSS version 20 for Windows (SPSS Inc., Chicago, Illinois, USA) and Microsoft Office Excel 2003 (Microsoft Corporation, Redmond, WA, USA).

3.3. Results

3.3.1. General Aspects

Each micro-CT dataset was composed of 512 images. The arterial network from the aortic bifurcation to the digital arteries of the toes was visible on four BS-R and four LO-M 3D reconstructions (Figure 1). Two injections failed (one BS-R and one LO-M). In both failed injections there was no evidence of vessel filling. Four out of five BS-G injections failed to fill the vessels and therefore no further analysis of the BS-G injected rats and cannulae was undertaken.

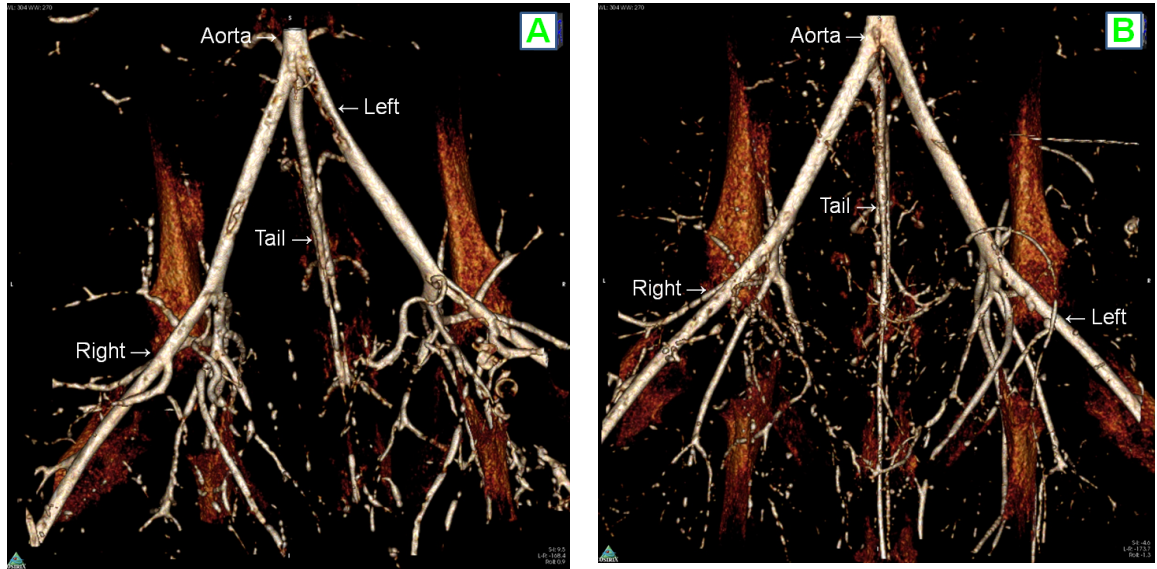


Figure 3.1. Anterior view of three-dimensional reconstruction images of the embalmed rat lower limb vessels injected with barium sulfate resin (A) and lead oxide milk powder (B) contrast media.

3.3.2. Quantitative and Qualitative Measurements

The number of continuous branching generations ranged from four to six (BS-R) and three to seven (LO-M). There was no significant difference (MD 0.05; MD 95% CI -0.83 to 0.93) between the number of branching generations of the rat lower limb vessels counted for the BS-R (mean 4.80; SE 0.30) and LO-M (mean 4.75; SE 0.34) (Table 1). The smallest vessel diameter visible on the rat arterial network 3D reconstructions was 0.07 mm for both the BS-R and LO-M preparations.

Table 3.1. Mean bias (95% CI) from low and high resolution micro-CT scan three-dimensional reconstructions, for cannulae of known ('true') internal diameter filled with barium sulfate resin or lead oxide milk powder.

Micro-CT Scan Resolution	Bias from known diameter, MD (95% CI)	
	Barium Sulfate (n=4)	Lead Oxide (n=4)
Low	0.03 (0.01 to 0.06)	0.03 (-.03 to 0.1)
High	0.05 (-0.04 to 0.14)	0.11 (-0.05 to 0.26)

3.3.3. Data analysis

The bias (mean difference) between the contrast medium and true cannula diameter was greater for LO-M (0.11 mm) compared to BS-R (0.03 mm) when the cannulae were scanned at high resolution (Table 3.1). At low resolution, the mean difference was the same for BS-R and LO-M. The variance of the estimates (1.96*standard deviation of the differences) was wider for LO-M compared to BS-R at both low and high resolutions (Figure 3.1). There was no significant difference (MD -.03; MD 95% CI -0.12 to 0.06) between the bias (known minus measured) for the BS-R (mean 0.04; SE 0.03) and LO-M (mean 0.07; SE 0.03). The ICC intra-observer (ICC_{3,1}) and inter-observer (ICC_{2,1}) reliability was excellent (Table 3.2).

Table 3.2. Reliability of the internal diameter measurements of the contrast-filled cannulae three-dimensional reconstructions.

Contrast	Intra-observer (ICC _{3,1})	Inter-observer (ICC _{2,1})
Barium	0.97	0.98
Lead	0.98	0.89

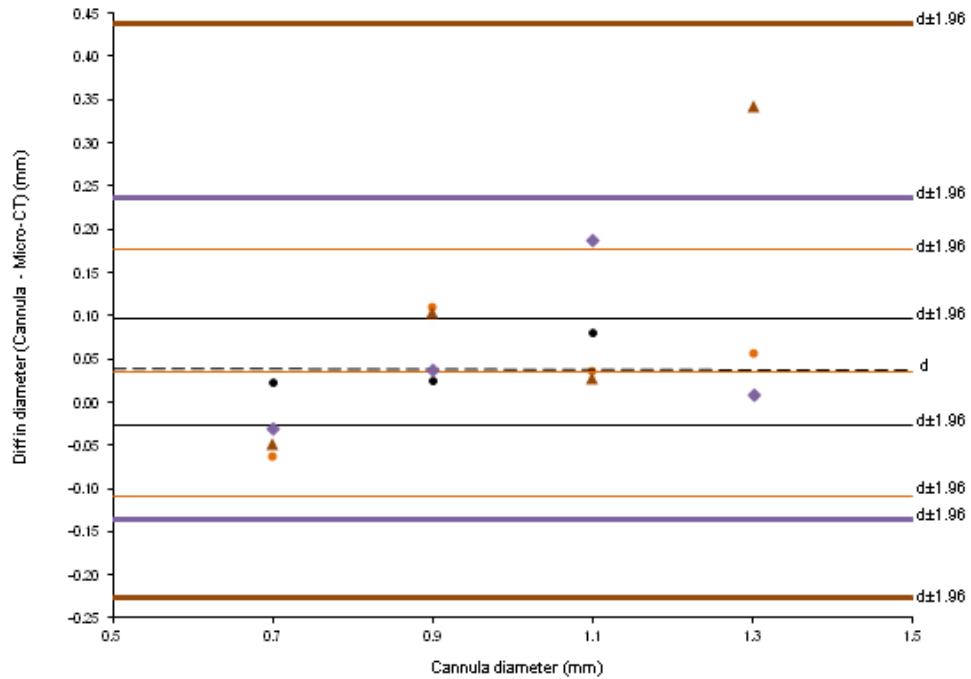


Figure 3.2. The mean difference (MD) and the variance of the estimates ($1.96SD = 1.96 \times \text{standard deviation}$ of the differences) between the lead oxide milk powder (grey) and barium sulfate resin (black) and known internal cannulae diameter when micro-CT scanned at high (thick line) and low (thin line) resolution ● - lead low resolution scan; ● - barium low resolution scan; ▲ - lead high resolution scan; ◆ - barium high resolution scan

3.4. Discussion

Barium sulfate resin (BS-R) was superior to lead oxide milk powder (LO-M) in terms of accuracy at high resolution and also in terms of reduced variance at both high and low resolution. Both media were equivalent in terms of extent of perfusion.

Barium sulfate is a non-toxic alternative contrast medium for micro-CT angiography. It has been used in previous studies but has not previously been assessed for accuracy compared to traditional standard preparations using lead oxide. Lead oxide supplanted barium sulphate as a contrast agent in the 1980s because it was believed to provide optimal visualisation of small vessels (Bergeron et al., 2006; Quinodoz et al. 2002). It was commonly combined with gelatin to prevent leakage. In this study we show for the first time that barium sulfate combined with resin represents both a safer and more accurate option.

Lead oxide demonstrated less accuracy at high resolution compared to barium sulfate. In this study we included both high and low scan resolutions in order to examine whether resolution altered the accuracy of our measurements. The relative decrease in accuracy at higher resolution in the lead oxide preparations was due to ‘scatter’ or ‘sun-burst’ artefact. Artefact of this type has been previously reported with lead preparations which are very high density (Tregakiss et al., 2007). The degree of artefact can be minimised by reducing the concentration of lead oxide. Tregaskiss et al. (2007) reduced the concentration of lead oxide by 66% compared to that previously used by Rees and Taylor (1986) for x-ray

studies, in order to minimise the artifact. They used a gelatin preparation with a lower concentration of lead (65 g PbO per 100 ml H₂O) compared to that used in this study (100 g Pb₃O₄ per 60 ml H₂O). Tregasskis et al. (2007) reported that this concentration was optimal for preventing artefact, however, in this study we employed a technique established for use in embalmed specimens, which was developed for x-ray angiography. It is possible that a lower concentration of lead oxide would have yielded better results. However, by not using lead oxide the problem is avoided altogether.

Lead oxide is not an ideal material to be used in the anatomical research and teaching environment for a number of reasons. The most important consideration is toxicity. Lead oxide is highly toxic and therefore requires PPE and specialist disposal (Bergeron et al., 2006). So, although lead oxide is cheaper to buy, this advantage is offset by the expense of disposal. Further, if lead oxide is used in a cadaveric specimen for imaging purposes it is rendered useless for further research or teaching. It is therefore preferable to use a preparation like barium sulphate and resin which, although more expensive, is safer and actually enhances the specimen for visualisation of the vessels for teaching.

In this study the barium sulfate and gelatine injections failed due to incomplete filling of the vessels but the reason is not clear. Solidification and blockage of fine gauge needles has been previously reported (Suami et al., 2007). Therefore it is possible that the fine vessels targeted in this study were too small for the gelatine preparation to penetrate. Barium sulfate and gelatine injections have previously been used with success in fresh cadavers (Bergeron et al., 2006). It is possible that the vessels in our embalmed specimens lacked

sufficient elasticity to allow adequate ingress. Gelatine is used to prevent leakage (Tregakiss et al., 2007) but resin also performs this function. It is therefore suggested that gelatine preparations are potentially less suitable for use in embalmed specimens.

The extent to which a contrast agent perfuses into the vessel tree is indicative of its utility for micro-CT angiography. No previous studies have compared contrast preparations for use in micro-CT angiography. In fresh human cadavers injected and scanned with conventional CT scanners (Tregakiss et al., 2007, Bulla et al., 2014), the smallest vessel measured was 0.4 mm (lead oxide gelatine), and 0.3 mm (barium sulfate resin) (Tregakiss et al., 2007, Bulla et al., 2014). In this study the smallest vessel diameter measured was 0.07 mm for both barium sulfate resin and lead oxide milk powder preparations. This increase in ability to visualise smaller vessels is unsurprising given the better resolution offered by micro-CT compared to conventional CT. However, the ability to visualise the small vessels depends on both the contrast agent and the substance in which it is suspended. We used milk powder and water to suspend the lead oxide because it has been successfully used previously in embalmed specimens (Suami et al., 2007). Similarly, barium sulfate mixed with resin has also been used previously but it is not clear whether the specimens were embalmed (Bulla et al., 2014). We have demonstrated that both contrast preparations were able to perfuse far enough into the vascular tree to take advantage of this new technology.

The technique used in this study demonstrated less bias than has previously been reported. Tregaskiss et al (2007) reported a mean difference in known glass tube length of 0.2 mm with variability of 2.28 mm. In this study barium sulfate resin produced the most accurate

results with a mean difference of 0.03 mm and variability of 0.27 mm. Therefore, anatomical examination of microvasculature is significantly enhanced by the use of micro-CT together with a barium sulfate resin contrast medium.

There are a number of limitations to this study. We used a small number of rats in each arm of the study, however, this is consistent with similar previous studies (Tregakiss et al., 2007, Bulla et al., 2014; Suami et al., 2007). A limitation of using micro-CT is that the resolution is inversely proportional to the size of the specimen i.e. the higher the resolution required the smaller the field of view therefore a smaller sample size is accommodated. Although the technology is improving rapidly and larger sample sizes are being accommodated, at this time longer scanning times are required.

3.5. Conclusion

In this study barium sulphate-resin and lead oxide milk powder preparations were compared for efficacy when visualising microvasculature using micro-CT in embalmed specimens. We found that barium sulfate combined with a low viscosity resin provided superior results at high resolution and was equivalent to lead oxide and milk powder in terms of extent of perfusion. We therefore recommend barium sulfate resin as an effective contrast preparation when assessing embalmed cadaveric microvascular anatomy using micro-CT due to its non-toxicity and minimal artefact at higher resolutions. The findings of this study were used to inform the study described in the next chapter. In this study barium

sulfate in low viscosity resin was used to investigate the intra-tendinous arterial supply of gluteus medius and minimus in embalmed human cadaveric specimens.

Chapter 4:

Vascular Imaging Studies

Chapter 4: Vascular Imaging Study.

4.1. Introduction.....	70
4.2. Methods	72
4.2.1. Exploratory Dissection Study	72
4.2.2. Cadaveric Specimens	72
4.2.3. Contrast Media Preparation.....	73
4.2.4. Specimen Preparation.....	73
4.2.5. Contrast Media Injection	74
4.2.6. CT Scanning	75
4.2.7. Dissection for Micro-CT.....	75
4.2.8. Micro-CT Scanning	77
4.3. Results.....	78
4.4 Discussion.....	83

4.1. Introduction

Micro-computed tomography (micro-CT) potentially offers a unique opportunity for high-resolution images of microvascular structures (Zagorchev et al., 2010). The use of micro-CT to investigate vascular anatomy is an emerging field, which has been used in both clinical and research settings (Tregaskiss et al., 2007; Chen et al., 2011; Gregor et al., 2012). Unlike clinical computed tomography (CT) imaging, micro-CT angiography can only be undertaken *ex vivo* in small animals and human tissues because of the higher radiation exposure, small scanner capacity and longer scanning times (Gregor et al., 2012).

Micro-CT angiography has been used to image vascular microarchitecture within the brain, kidney, heart and blood vessels in small animal models only (Schambach et al., 2010; Ghanavati et al., 2014). Tregaskiss et al. (2007) used conventional CT angiography to image the vasculature and micro-vasculature of the anterior abdominal wall. However, a significant limitation of the three-dimensional (3-D) CT angiography method that they used was that it was unable to visualise vessels less than 0.4 mm in diameter and the limits of agreement were greater than 1 mm (Tregaskiss et al., 2007). Therefore, this method would not allow reliable visualisation of very small vessels such as arterioles.

Previous arterial anatomy studies of the lower limbs have used CT angiography relying on iodine contrast in in-vivo patient based CT scans and investigated the origins and branching of arteries (Basar et al. 2002; Fukada et al., 2005). Other options for arterial investigations of surgical flaps, blood supply of femoral head and tendinous arterial supply are based on

cadaveric dissection, histological and/or angiographic studies (Rees and Taylor, 1986; Chen et al., 2009; Zlotorwicz et al., 2012; Vegas and Martin-Hervas, 2013).

This thesis is concerned with investigating the micro-vasculature in the gluteal tendons. These vessels have been described as arterioles, which are reported to range between 30 – 100 μm in diameter (Koeppen & Stanton, 2017) . Micro-CT angiography has been reported to achieve a resolution of 24 μm in mouse lower limbs (Zagorchev et al., 2010). Therefore, micro-CT is theoretically a good imaging method for visualising intratendinous vasculature. However, there are no published data describing micro-CT angiography in tendons to date.

The ability to image vessels is highly dependent on the contrast medium. In recent years, barium sulphate and lead oxide contrast media have commonly been used to investigate micro-vasculature (through X-ray and micro-CT angiography) due to the increased detail of the images produced and ease of use (Rees and Taylor, 1986; Bergeron et al., 2006; Tregakiss et al., 2007). However, other contrast agents have been investigated for use with non-vascular micro-CT. Pauwels et al. (2013) studied 28 different contrast agents (including barium, lead, iron, copper, potassium, mercury, sodium and silver compounds). Their evaluating of differential contrast enhancement between muscle and adipose tissues and differentiation between different soft tissue groups, demonstrated no distinctively superior contrast media found.

In Chapter 3 we investigated barium sulphate in a resin suspension in embalmed rats. In this study, we used this methodology in embalmed human cadaveric specimens to investigate the blood supply to the lateral hip, and in particular, the gluteal tendons.

The aims of this study were to:

1. Investigate the penetration of a barium sulphate contrast media in embalmed human cadavers with CT and micro-CT
2. To investigate if contrast-filled micro-vessels can be visualised within tendons using micro-CT angiography
3. To investigate the origins of the lateral circumflex femoral artery (LCFA) and medial circumflex femoral artery (MCFA) using micro-CT 3-D reconstructural imaging

4.2. Methods

4.2.1. Exploratory Dissection Study

A dissection study was performed to investigate the vascular anatomy and determine the optimal contrast injection site.

For details of the dissection study see Appendix 1.

4.2.2. Cadaveric Specimens

Eleven hip and lower limb specimens were removed from six embalmed cadavers (3 males and 3 females, aged 58 – 93 years, 6 left and 5 right). These cadavers had been embalmed

with Genelyn Arterial Solution (GMS Innovation, Adelaide, South Australia) through either the femoral or radial arteries. If the femoral artery had been used for embalming, this site was then inspected for any torn or transected vessels. Any damaged vessels, other than the circumflex femoral arteries, were tied with 2-0 vicryl sutures (Ethicon Inc, Somerville, United States). All toes were transected to ensure complete filling of the vessels. This study was approved by the ACT Health Human Research Ethics Committee (ETHLR.14.074) and the Australian National University Human Ethics Committee (A2014/080)

4.2.3. Contrast Media Preparation

The barium sulphate resin (BS-R) contrast media was prepared as per the methods in 3.2.2.1.

4.2.4. Specimen Preparation

The cadaveric specimens in this study had been transected proximal to the bifurcation of the aorta. It was noted that there was thrombosis and atherosclerosis within the common iliac vessels of each specimen. The issue of thrombosis and atherosclerosis was addressed by physically removing as much as possible through the cut proximal ends of the vessels with artery forceps.

A 50 ml syringe was used to inject the 6% hydrogen peroxide solution into the aorta to identify any leaks from the vessels, which were then covered with superglue. With

Specimens 3 and 4, the microvascular filling was attempted to be improved by covering the distal cut ends with epoxy resin. This resulted in markedly increased pressure and a decrease in the amount of contrast media able to be injected. Therefore, the distal cut ends of the specimens were re-sectioned to allow the contrast media to move more freely through the system so that a further 20 ml could be introduced. All subsequent specimens were injected with open distal vessels.

4.2.5. Contrast Media Injection

The contrast media was injected into the vessels using a 50 ml syringe in a pulsatile manner until the contrast was seen to be leaking from the distal cut ends of the vessels. The specimens were injected at different sites. The first four specimens were injected through the cut end of the aorta proximal to its bifurcation. However, due to the suboptimal filling of the circumflex and gluteal vessels, which was assessed from the CT images, the injection site was altered for subsequent specimens. Specimens 5 through 8 were injected through the cut proximal ends of the internal and external iliac arteries at increasingly more distal levels in an attempt to improve vessel filling. In Specimens 10 and 11, the external iliac artery was injected just proximal to the inguinal ligament, whilst the internal iliac artery was injected as distal as possible to its origin before traversing through the sciatic foramen.

After injection, the contrast media was then left to set at least overnight. The hips were then double-bagged and vacuum-sealed for storage and transport to the scanning site.

4.2.6. CT Scanning

Each specimen was scanned using a Toshiba Aquilon Prime Computerized Tomography Scanner (Toshiba Medical Systems Corporation, Tochigi, Japan). These macro-images were taken because of the limited field of view of the micro-CT. The macro-images allowed for the identification of the source vessels. Each micro-CT image was viewed in the context of the macro image.

Each hip specimen was positioned supine in the CT scanner with the distal aspect closest to the scanner for consistent alignment. The scanning sequence parameters were: 120 kV, 259 mAs, slice cut thickness of 0.5 mm with an inter-slice gap of 0.4 mm. Three-dimensional reconstructions of the CT were created using Syngo Imaging VB36D (Siemens AG, Muechen, Germany). The origin and extent of contrast filling of the gluteal and circumflex femoral arteries were determined from the CT images.

4.2.7. Dissection for Micro-CT

After CT scanning the specimens were further dissected to reduce the length to less than 18 cm to comply with the constraints of the micro-CT scanner. This dissection removed the skin, adipose tissue, gluteus maximus and sacrum. All dissected hip specimens retained the proximal and distal attachments of gluteus medius and minimus. The boundaries of the specimen were defined by the anterior superior iliac spine, posterior inferior iliac spine and 1 cm distal to the lesser trochanter.

To map the micro-CT data to corresponding histological sections (Chapter 5), 2-0 vicryl sutures were placed as markers. A running stitch was made longitudinally along gluteus medius from the anterior aspect of the greater trochanter (GT) to the proximal portion of the specimen. Further 2-0 vicryl sutures were then placed horizontally, perpendicular to the longitudinal suture, at 5 mm intervals along the gluteal tendon/muscles from the tip of the GT proximally for 4 cm, and then at 1 cm intervals for 5 cm as shown in Figure 4.1.

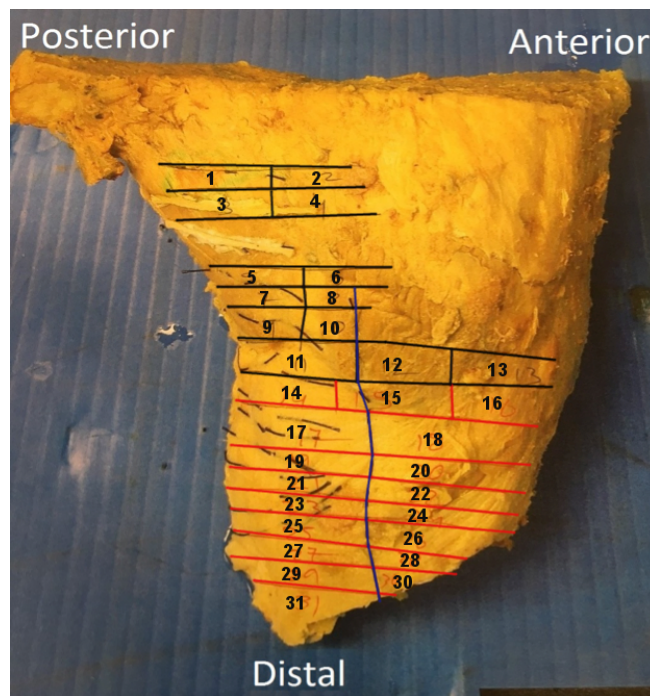


Figure 4.1. Lateral view of Specimen 3, showing correlation of slide number to specimen prior to histological sectioning. black lines - slides within muscle; red lines - slides within tendon; blue lines - line along anterior aspect of greater trochanter

4.2.8. Micro-CT Scanning

The cadaveric specimens were scanned using a Heliscan micro-CT scanner (Australian National University, Canberra, Australia). The hips were double-bagged, vacuum-sealed and placed upright within the scanner. They were held in place with a bespoke cylindrical plastic container on an aluminium stand. The sequence parameters for each specimen are described in Table 4.1.

Table 4.1. Micro-CT Scanning Parameters.

Specimen	FOV	Voxel Size	kV	μ A
1	183.1	62.71	100	105
2	202.7	72.39	120	100
3	183.9	62.96	100	105
4	152	54.29	120	100
5	208.8	74.56	100	120
6	208.8	74.56	100	120
7	179.6	64.13	100	120
8	184.7	65.96	120	120
9*		N/A		
10	224.9	77.02	120	120
11	233.8	80.06	120	120

Note. * Specimen 9 was not scanned using micro-CT due to the presence of a total hip replacement visible on CT. FOV – Field of view; kV – kilovolt; μ A - microampere

Three-dimensional reconstructions of the micro-CT images were created using *Drishti: a volume exploration and presentation tool* (Australian National University, Canberra, Australia). The Drishti tool allows for segmentation of different tissues enabling the vascular components with contrast media to be viewed in isolation, and also in relation to surrounding bone and soft tissues.

4.3. Results

During CT scanning it was noticed that Specimen 9 contained a total hip replacement and was therefore excluded from the remainder of the study.

The lateral circumflex femoral artery (LCFA) and medial circumflex femoral artery (MCFA) were visible on all micro-CT 3D reconstructions, except for specimen 11 where the MCFA was not visualised (Figure 4.2). The LCFA originated from the profunda femoris artery (PFA) in all specimens whilst the MCFA branched from the PFA in 50% (5 specimens), femoral artery (FA) in 40% (4 specimens) and as a common trunk with the PFA in 10% (1 specimen) (Table 4.2).

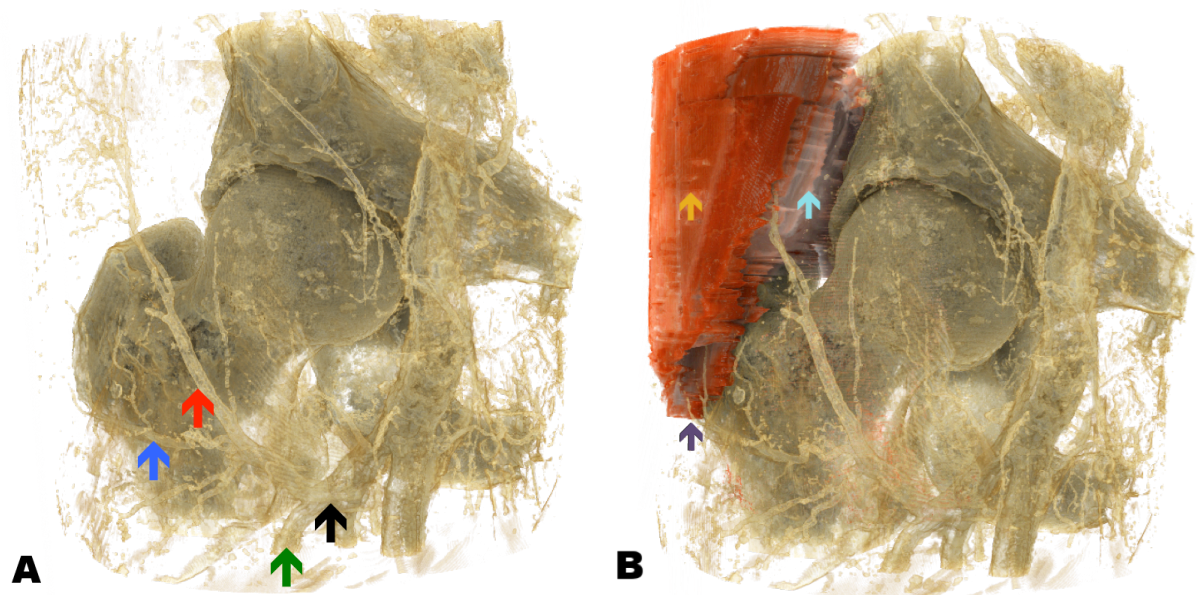


Figure 4.2. 3-D micro-CT reconstruction of the right hip (Specimen 5), anterior view, showing the hip joint and circumflex vessels (A), and in relation to the gluteus medius and minimus muscles (B). **↑** – lateral circumflex femoral artery (LCFA); **↑** – descending branch of LCFA; **↑** – ascending branch of LCFA; **↑** – transverse Branch of LCFA; **↑** - gluteus medius muscle; **↑** - gluteus minimus muscle; **↑** - gluteal tendons

Table 4.2 Origins of LCFA and MCFA as determined from the 3-D micro-CT reconstruction images.

Specimen	LCFA Origin	MCFA Origin
1	PFA	PFA
2	PFA	PFA
3	PFA	PFA
4	PFA	FA
5	PFA	FA
6	PFA	PFA
7	PFA	FA
8	PFA	Common Trunk with PFA
9	-	-
10	PFA	FA
11	PFA	Not Visualised

Note. FA – Femoral Artery; LCFA – Lateral Circumflex Femoral Artery; MCFA – Medial Circumflex Femoral Artery; PFA – Profunda Femoral Artery.

The contrast media completely filled the LCFA and partially filled the MCFA, however it was possible to identify the origins of their branches. The ascending branch (AB) and transverse branch (TB) branched from the LCFA as a common trunk in all but one specimen (Specimen 1), and the descending branch (DB) originated from the LCFA in all specimens.

The LCFA and MCFA branches were incompletely filled by the contrast medium (Figure 4.3; Table 4.3). The DB was filled to the limit of the image in all scans. Due to the partial filling of the MCFA the branches could not be visualised

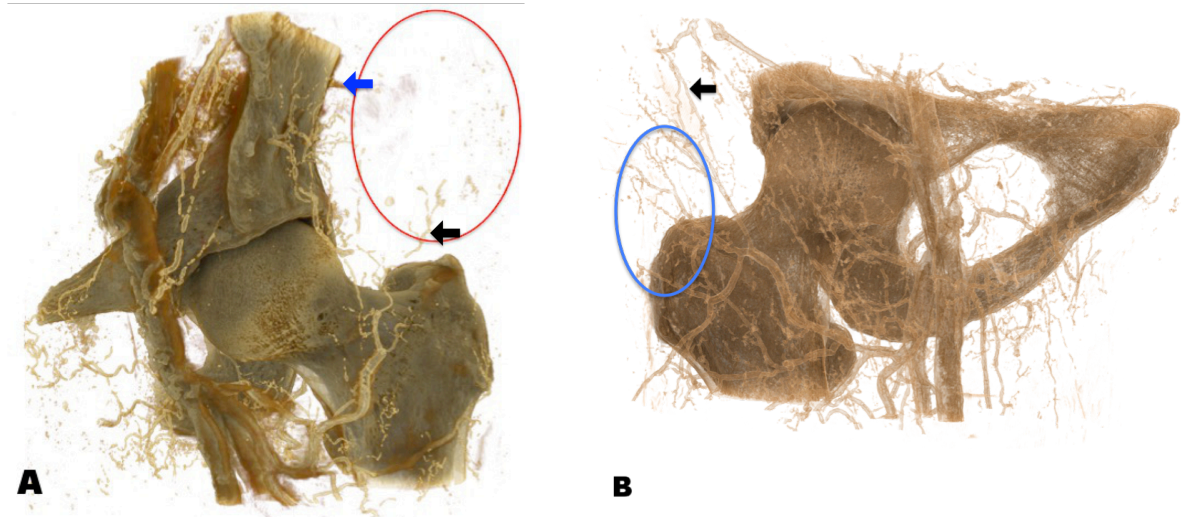


Figure 4.3. 3-D micro-CT reconstruction images showing the anterior view of the hip joint and contrast-filled vessels of Specimen 5 (left hip joint) showing incomplete filling of the terminal branches of IGA and AB of the LCFA (red circle) (A) and Specimen 8 (right hip joint), showing the area corresponding to the gluteal tendons and filled branches of AB and TB of the LCFA (blue circle) and the decreased field of view that does not visualise the IGA (B). ← - AB of LCFA - Ascending Branch of Lateral Circumflex Femoral Artery; ← - IGA - Inferior Gluteal Artery

Table 4.3. Most distal point of contrast media filling of the Ascending Branch and Transverse Branch of the LCFA.

Specimen	AB	TB
1	Middle of femoral neck	Midpoint of intertrochanteric line
2	Superior Femoral Neck	Medial base of femoral neck
3	Mid Femoral Neck	Lateral Femur
4	Superior Femoral Neck	Inferior portion of greater trochanter
5	Ilium*	Lateral Femur
6	Superior Femoral Neck	Mid Femur
7	Acetabulum*	Lateral Femur
8	Mid Femoral Head*	Mid Femur
9	-	-
10	Mid Femur	Mid Femur
11	Intertrochanteric Line	Mid Femur

Note. * - Indicates upper limit of scan image. LCFA – lateral circumflex femoral artery

To address the second aim of this chapter the 3-D reconstruction images were viewed from an axial view to assess if there were vessels within the gluteal tendons (Figure 4.4). No vessels were observed within either of the gluteal tendons in any specimens.

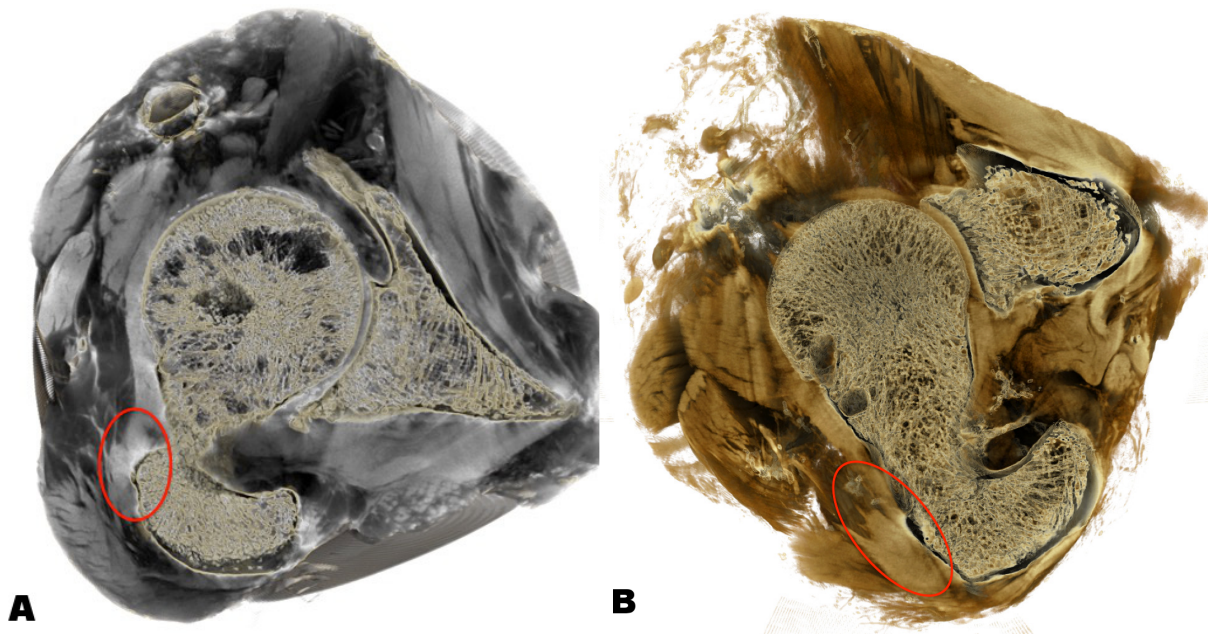


Figure 4.4. Superior axial 3-D micro-CT reconstruction images showing two left hip joints and contrast-filled vessels in relation to the gluteal tendons. A. The contrast-filled vessels are coloured gold and there are none within the gluteal tendon (red circle). B. Some contrast-filled vessels are visible external to the gluteal tendons but not within the tendon.

4.4 Discussion

The main finding of this study was that we were unable to visualize any intra-tendinous vessels in embalmed cadaveric hips using a micro-CT angiography method with barium sulphate contrast media.

There were three main aims for this chapter: to investigate the penetration of the barium sulphate contrast media into embalmed cadaveric vessels; to determine if contrast-filled

vessels can be seen within the gluteal tendons with micro-CT angiography; and to investigate the origins of the LCFA and MCFA.

Different levels of detail can be obtained with micro-CT depending on the contrast particle size and viscosity (Zagorchev et al, 2010). The contrast we used did not appear to adequately penetrate the small vessels in these specimens. There are two potential reasons for why this occurred. The first is that the penetration of the contrast in embalmed cadavers maybe affected by the presence of thrombus and atherosclerosis inside the lumen of the vessels. Although we removed the most proximal thrombus and atherosclerosis prior to injection of hydrogen peroxide this would not have cleared the lumen of the vessels down to the microvasculature. The preparation between the rats and cadavers differed, with the rats vascular system being flushed as they were embalmed (described in Chapter 3.2.1).

The second reason for inadequate penetration may have resulted from incomplete solution of the barium sulfate in the resin. It was clear that the powder was still visible regardless of the length of time or intensity of mixing. This may have resulted in blockage of the lumen in the microvasculature. The procedure for preparing the barium sulfate resin contrast did not differ from the contrast comparison study in Chapter 3. Therefore the incomplete clearance of the lumen of the vessels may have been a more important factor.

The anatomical findings of this study were not entirely consistent with previous descriptions. The LCFA originated from the PFA in all cases in this study. However, in

previous studies the LCFA originated from the PFA in 70 – 83% of specimens (Lipshutz, 1916; Adachi, 1928; Xu et al., 1989; Heitmann et al., 1998; Dixit et al., 2001; Vazquez et al., 2008; Uzel et al., 2008; Tansatit et al., 2008; Prakash et al., 2010; Dixit et al., 2011; Kalhor et al., 2012; Sinkeet et al., 2012; Anwer et al., 2013; Peera and Sugavasi, 2013; Anjankar et al., 2014; Manjappa and Prasanna, 2014; Nasr et al., 2014). In this study the origin of the MCFA was from the PFA in 40% specimens and the FA in 40%. This compares to 60 – 83% from the PFA and 6.4 – 40% from the FA reported in the literature (Lipshutz, 1919; Adachi, 1928; Clarke and Colburn, 1993; Gautier et al., 2000; Dixit et al., 2001; Tanyeli et al., 2006; Prakash et al., 2010; Zlotorowicz et al., 2011; Kalhor et al., 2012; Anwer et al., 2013; Lalovic et al., 2013).

Variation of the arterial networks are thought to be established in the embryo around the 13 mm stage (Senior, 1924). At this stage the embryonic vessels consist of a primary arterial trunk or “axis” and the “rete femoralis” or capillary network (Senior, 1924; Keen, 1961). Variations in the arterial configuration are thought to be due to the persistence of embryonic vessels (Keen, 1961). It is thought that there may be a genetic contribution to the configuration of the variations but this is not yet clear (Keen, 1961).

There were a number of limitations in this study. The first was the use of embalmed specimens, which most likely limited the penetration of the contrast medium. The second was the small number of specimens because the resultant data may not have accurately represented the percentage of anatomical variations.

In conclusion, we were unable to confirm that micro-CT angiography using barium sulfate resin is an effective method for assessing intra-tendinous arterial supply in embalmed human cadaveric specimens. Further studies should be made in fresh hip specimens to determine whether micro-CT is effective in the absence of thrombus and atherosclerosis. In the next chapter micro-CT angiography will be compared with histology to determine if intra-tendinous arteries not visible on micro-CT are present in the gluteal tendons.

Chapter 5:

Histological Study

Chapter 5: Histological Study.

5.1. Introduction.....	89
5.2. Methods	92
5.2.1. Techniques for Matching Micro-CT to Histology	93
5.2.2. Histological Assessment.....	94
5.3. Results.....	97
5.3.1. Vessels.....	98
5.3.2. Tendon Degeneration	101
5.3.3. Muscle Degeneration.....	103
5.4. Discussion.....	106

5.1. Introduction

Histology provides the most robust method for determining the vascularity of tendons. A normal tendon is comprised primarily of collagen bundles arranged in a hierarchical organization, increasing in complexity of structure. The tendon is covered by the epitenon, which extends between the bundles of collagen fibres as the endotenon (Khan et al., 1999). Surrounding the epitenon is the paratenon, which is a layer of loose connective tissue, mostly comprised of type I and III collagen fibrils, elastic fibrils and synovial cells (Khan et al. 1999). A pictorial description of these layers is shown in Figure 5.1. The collagen bundles and surrounding layers of epitenon and paratenon are able to be analysed using histological methods (Khan et al., 1999).

Tendon vascularity is not well understood. Although tendons are often thought to be avascular, evidence of small arteries or arterioles have been observed within tendons (Khan et al., 1999; Cheng et al., 2010). The direction of the arteries has been reported to be longitudinal, either within or surrounding the tendon (Brooks et al., 1992; Khan et al., 1999). Intra-tendinous vessels have been visualised within the Achilles, patella, supraspinatus, tibialis posterior and long head of biceps tendons (Brooks et al., 1992; Ahmed et al., 2002; Petersen et al., 2002; Pang et al., 2009; Cheng et al., 2010). In the flat tendons (patella and supraspinatus) the vessels course through the whole length of the tendon, running mostly in a longitudinal direction (Rathbun & MacNab, 1970). In contrast, in round tendons (Achilles, posterior tibial and long head of biceps tendons) the vessels are derived from the paratenon and enter the substance of the tendon at intervals along its length (Rathbun & MacNab, 1970).

The size of intratendinous vessels has not been well reported. Only Brooks (1992) reported the diameter of intra-tendinous vessels. The supraspinatus tendon vessels were between 30 μm – 50 μm , decreasing in size in the last 30 mm of the tendon before its humeral attachment. The intra-tendinous vascularity of the gluteal tendons has not previously been described.

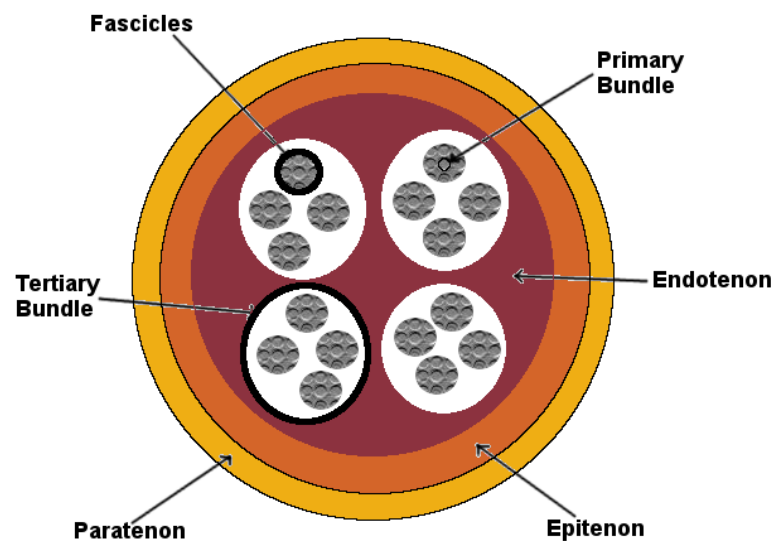


Figure 5.1. Cross-sectional representation of a tendon, showing the internal fascicles and tendon bundles and the outer layers (epitenon and paratenon).

Pathological changes to tendons cause dysfunction of the muscular unit due to pain, offloading, and decreased use (Gibbons et al., 2017). This dysfunction can lead to atrophy, scarring and fatty infiltration in the muscle proximal to the pathological tendon (Gibbons et al., 2017). With regards to gluteus medius, fatty infiltration has been found within the

anterior and mid-anterior portions of the muscle in elderly embalmed cadavers, both with and without gluteal tendon tears (Flack et al., 2013; Takano et al., 2018). This process of fatty infiltration into muscle is unclear if it is a normal aging or a pathological process (Flack et al., 2013; Takano et al., 2018).

Histological examination is traditionally undertaken by staining and sectioning the tissue, then visualising the structures under a microscope. However, this technique results in the specimen being destroyed and the relative positions of the structures being disrupted (Zagorchev et al., 2010). Micro-computed tomography (micro-CT) is potentially a better method allowing visualisation of vessels within intact tissue (Zagorchev et al., 2010). Using contrast agents with micro-CT has enabled the production of 3-dimensional (3-D) images, preserving spatial relationships and increasing the ability to evaluate soft tissue structures and vessel morphology (Schambach et al., 2010). However, although vessels have been imaged with micro-CT there have been no studies investigating intra-tendinous vascularity.

This study has two aims:

1. To investigate and describe the intra-tendinous vascularity of the gluteal tendons, including all tendinous layers.
2. To compare the accuracy of micro-CT with histology for identifying and quantifying intra-tendinous vessels in the gluteal tendon.

5.2. Methods

After completion of micro-CT scanning (previously described in Chapter 4.2.5), the ten cadaveric specimens were further dissected to allow for decalcification and histological sectioning along the marking sutures (previously described in Chapter 4.2.2). The ilial and greater trochanteric attachments of gluteus medius and minimus muscles were kept intact to preserve the gluteal tendons. For the purpose of this study the tendons were considered as a single unit.

All the embalmed specimens containing bone and tendon were placed in 50 mL of sterile buffered 10% formalin for 24 hours. Once fixed with buffered 10% formalin, the specimen was then sectioned at the marking sutures as described in 4.2.4 (Figure 5.2).

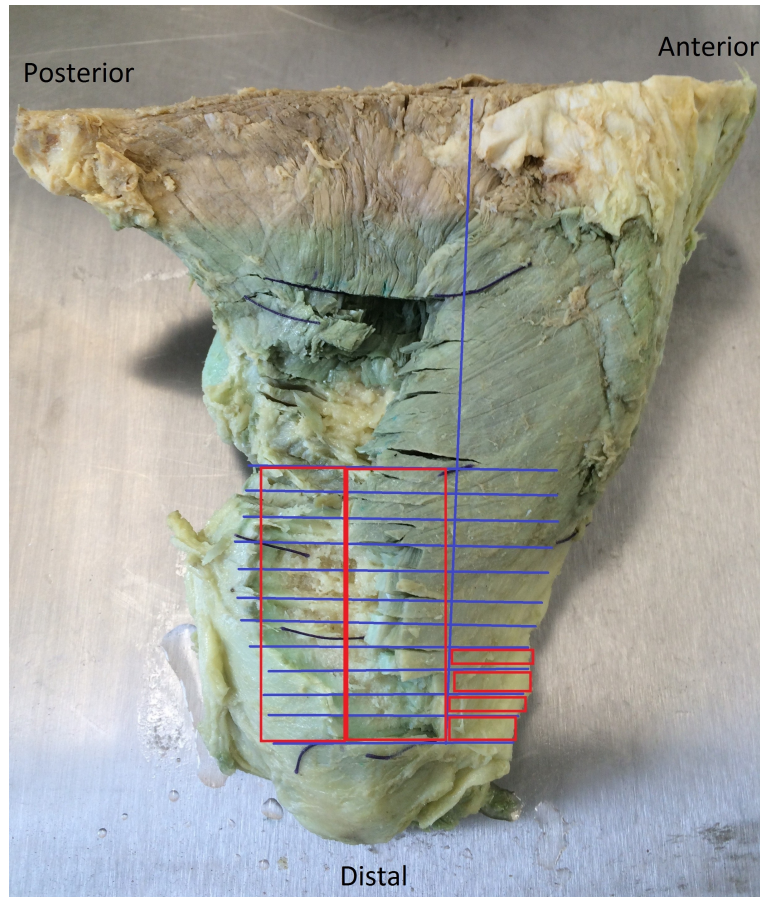


Figure 5.2. Lateral view of right gluteal muscles of Specimen 1. The marking sutures are overlaid with the grid pattern used to plan the histological section. In this figure the blue lines indicate the marking suture levels and the red squares indicate the location of the gluteal tendons.

The sections containing bone were decalcified in 5% nitric acid for between seven to ten days. The sections were then placed into formalin for a further hour, dehydrated, embedded in paraffin, and cut in 4 μm slices with a microtome and stained with Haematoxylin and Eosin (H&E). The slides were then viewed under a BX23 light microscope (Olympus, Notting Hill, Australia) using up to thirty times magnification to assess for intra-tendinous arteries from proximal to distal along the length of the tendons.

This study was approved by the ACT Health Human Research Ethics Committee (ETHLR.14.074) and the Australian National University Human Ethics Committee (A2014/080)

5.2.1. Techniques for Matching Micro-CT to Histology

The challenge with undertaking a comparative study of micro-CT and histology is to accurately match the images, since the specimen is destroyed during preparation for histology. To achieve a comparison, the position of the histological slices were mapped to the micro-CT image of the whole specimen as suggested by Zagorchev et al. (2010).

Suture material was placed horizontally along the length of the tendon on the outside of the specimen (Figure 4.1) for direct comparison with histology sectioning as described in 4.2.7. The histological sectioning of the specimen was undertaken along these sutures and it was hypothesised that these sutures would be able to be visualised on the 3-D reconstruction, allowing for comparison of the same slice of specimen across the two different methods.

5.2.2. Histological Assessment

Assessment of the histological slides was made by a pathologist with 5 years experience, who reviewed each slide and created a table which summarised the presence, size and location of the arteries. Independently, the researcher completed the same table for the axial micro-CT reconstructions undertaken on Drishti. These findings were subsequently compared by direct comparison of the position of the vessels on axial micro-CT reconstructed images with those within the histological table and slides.

Whilst the histological slides were visualised under the light microscope, there were particular features of the tendons that were analysed. The presence of any arteries/arterioles and evidence of changes related to tendon degeneration were noted for all tendinous layers within slides that contained tendon. Tendon degeneration was assessed in order to understand whether there was a relationship between degeneration and increased or decreased vascularity. The specific histopathological changes for tendon degeneration were based from the modified Bonar score (Fearon et al. 2014) and included semiquantitative measures of the following five parameters: cellular morphology, collagen arrangement, cellularity, vascularity and ground substance (Table 5.1).

The highest possible score on the modified Bonar score is 20, with each of the five categories being rated from 0 - 3 and then a further 2.5 points added for each of calcification and intratendinous adipocytes (Fearon et al. 2014). However, neither of calcification or intratendinous adipocytes were assessed in this study, allowing a maximum score of 15 based on the five categories.

Table 5.1. Bonar score adapted from Fearon et al. (2014)

	Grade 0	Grade 1	Grade 2	Grade 3
Cell Morphology	Inconspicuous elongated spindle shaped nuclei with no obvious cytoplasm at light microscopy	Increased roundness: nucleus becomes more ovoid to round in shape without conspicuous cytoplasm	Increased roundness and size; the nucleus is round, slightly enlarged and a small amount of cytoplasm is visible	Nucleus is round, large with abundant cytoplasm and lacuna formation (chondroid change)
Collagen arrangement	Collagen arrangement in tightly cohesive well marked bundles with a smooth dense bright homogenous polarisation pattern with normal crimping	Diminished fibre polarisation: separation of individual fibre bundles but with maintenance of overall bundle architecture	Bundle changes: separation and loss of demarcation of fibre bundles, giving rise to expansion of the tissue overall and clear loss of normal polarisation pattern	Marked separation of fibre bundles with complete loss of architecture
Cellularity	Mainly discrete cells	Hyper cellular, in runs and/or increased cell numbers	Areas of hypo as well as hyper cellularity	Area of assessment is mostly acellular
Vascularity	Inconspicuous blood vessels coursing between bundles	Occasional cluster of vessel, <2 per 10 hpf	2-3 clusters of capillaries per 10 hpf	Areas with >3 clusters per 10 hpf, and/or areas of pathological avascularity
Ground Substance	Not stainable ground substance	Stainable mucin between bundles but bundles still discrete	Stainable mucin with bundles with loss of clear demarcation of bundles	Abundant mucin throughout the section with inconspicuous collagen staining

Note – hpf – high power field

Muscle degeneration² has been found to occur with advanced tendon disease within the rotator cuff (Gibbons et al. 2017). Muscle degeneration was evaluated according to five morphological criteria derived from Rüegg and Meinen (2014). These criteria included:

1. Percentage muscle tissue replaced by fibrotic and adipose tissue.
2. Presence of irregular shaped myocytes - degenerating myocytes have irregular shape and few nuclei.
3. Central nuclei - myofibres with central nuclei indicate that the muscle fibre is in the process of regeneration.
4. Presence of inflammatory cells - inflammatory cells infiltrating damaged muscle fibres are indicative of secondary inflammation.
5. Heterogeneous fibre distribution – normal muscle has homogenous fibre size distribution but muscle undergoing repeated cycles of de-/regeneration has both small and large fibres.

Both the proximal and distal muscle tissue was assessed and compared. The proximal muscle was taken from the most proximal 20 mm of muscle; and the distal muscle was taken from the muscle within 20 mm of the musculotendinous junction.

² Muscle degeneration is defined as the presence of hypercellular infiltration of muscle fibres, the disruption of the integrity of the muscle fibre membrane or split muscle fibres (Gibbons et al. 2017)

5.3. Results

5.3.1. Vessels

There were no arteries or arterioles seen within tendon on any micro-CT images or histological slides. There was a single vessel measuring between 0.2 and 0.25 mm (correlated to a small arteriole) within slides 1 – 8 of each specimen, which, as per figure 5.3, corresponds to the muscular portion of the specimens. In some specimens, this single vessel was observed as distal as slide 14 (corresponding to the muscle and musculotendinous junction) as shown in figure 5.2. However, there were no arteries or arterioles of this size or smaller seen in slides distal to slide 14 in any specimen.

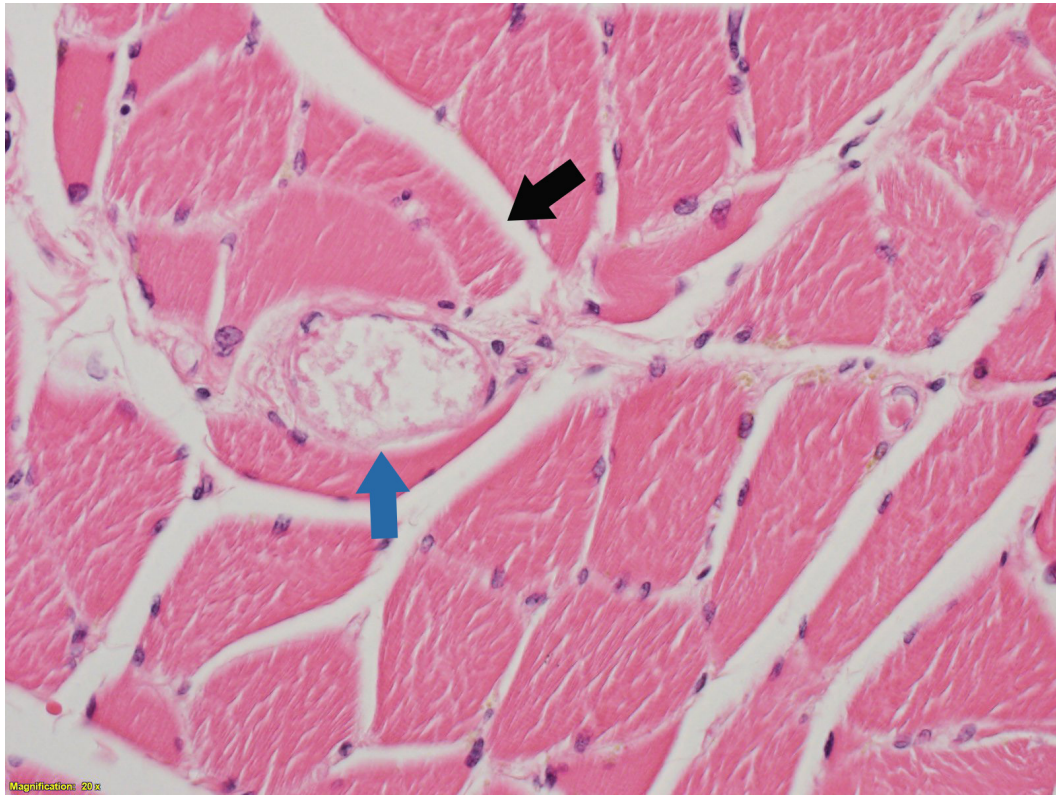


Figure 5.3. Proximal histological slide (slide 8, cross-sectional cut) of Specimen 8 viewed at 20 x magnification,  - single blood vessel,  – muscle fibre.

The only vessels that were viewed within the tendon were capillaries around the enthesis³. These occurred in all specimens except for specimen 1 and 3, as shown in Figure 5.5.

³ An enthesis is the area in which a tendon attaches to bone, it is made up of four zones from proximal to distal: tendon, fibrocartilage, calcified fibrocartilage and bone (Benjamin et al. 1986; Benjamin et al. 2002)

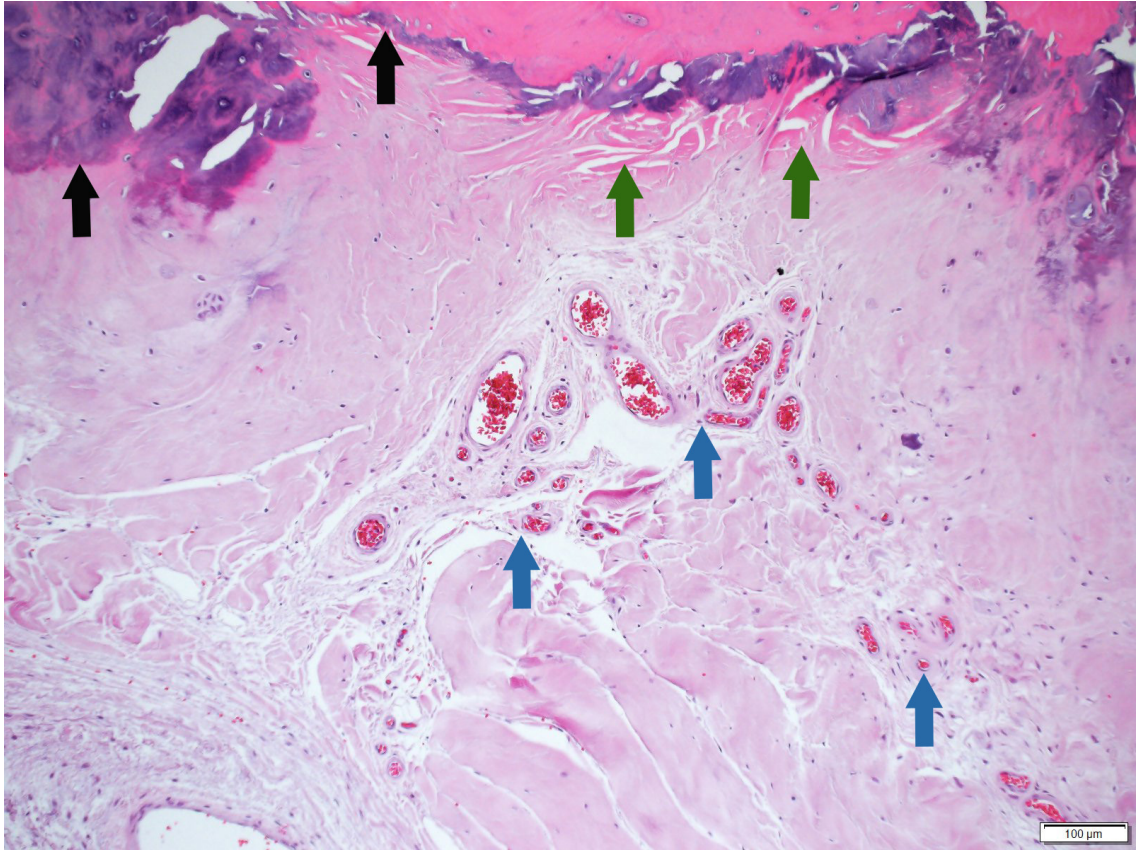


Figure 5.4. Neovascularisation of enthesis in histological section of Specimen 11 (slide 15, cross-sectional cut), viewed at 10 x magnification, **↑** - areas of neovascularisation, **↑** - enthesis, **↑** - degenerative tendon at the enthesis.

Table 5.2. Position of vessels associated with the gluteal tendons.

Specimen (side)	Muscle		Tendon		Distance
	Paratenon	Epitenon	Enthesis	Neovascularisation to entheses	
1 (R)	1 arteriole in slides 1 - 9	No vessels	No vessels	No vessels	N/A
2 (L)	1 arteriole in slides 1 - 10	No vessels	Slide 15-19	Neovascularisation slides 11-19	100 μ m
3 (R)	1 arteriole in slides 1 - 14	No vessels	No vessels	No vessels	N/A
4 (L)	1 arteriole in slides 1 - 9	No vessels	Slides 11-13	Neovascularisation slides 10-19	At Enthesis
5 (R)	1 arteriole in slides 1 - 12	Slide 15	Slides 15-18	Neovascularisation slides 12-22	At Enthesis
6 (L)	1 arteriole in slides 1 - 13	Slides 13-14	No vessels	Neovascularisation slides 14-24	2 mm
7 (R)	1 arteriole in slides 1 - 13	Slides 14-17	No vessels	Neovascularisation slides 14-21	0.5 mm
8 (L)	1 arteriole in slices 1 - 13	Slides 14-17	Slides 15-18	Neovascularisation slides 14-21	1 mm
10 (R)	1 arteriole in slides 1 - 10	No vessels	Slides 13-15	Neovascularisation slides 11-19	0.5 mm
11(L)	1 arteriole in slides 1 - 10	No vessels	Slides 11-13	Neovascularisation slides 11-19	At Enthesis

Note. μ m – micrometres, mm - millimetres

5.3.2. Tendon Degeneration

It was found that degeneration within the tendon was seen to increase distally. The highest score was reported for each specimen, shown in Table 5.3. The modified Bonar scores ranged from 4 – 10 out of a possible 15.

Table 5.3. Modified Bonar score for the most degenerative histological slide of each specimen.

Specimen	Cell Morphology	Fibre Arrangement	Cellularity	Vascularity	Ground Substance	Total
1	1	1	1	1	1	5
2	0	1	3	2	1	7
3	1	1	1	0	1	4
4	0	1	2	2	1	6
5	0	1	3	1	1	6
6	0	0	3	1	1	5
7	2	2	2	2	2	10
8	0	1	2	0	2	5
10	2	1	1	1	1	6
11	0	1	1	1	1	4

Note - The modified Bonar score was adapted from Fearon et al. (2014). The modified Bonar score for this study is a scale from 0 (normal tendon) – 15 (greatest abnormality detectable).

5.3.3. Muscle Degeneration

An unexpected, yet interesting finding was that there was evidence of degeneration (fibrous and fatty connective tissue) in the muscle fibres within the specimens. These changes were divided into proximal and distal muscular portions to further assess where within the muscle this degeneration occurs (Tables 5.4 and 5.5). Within the proximal musculature, five out of the ten specimens showed degenerative changes. Degenerative changes were found within the distal musculature of all ten specimens.

Table 5.4. Changes in muscle in proximal portion of specimen

Specimen	% Fibrous and fatty connective tissue	Irregular round shaped myocyte	Myocyte with central nuclei	Inflammatory cells	Heterogenous fibres distribution
1	5%	absent	absent	absent	absent
2	absent	absent	absent	absent	absent
3	10%	absent	absent	absent	absent
4	5%	absent	absent	absent	absent
5	absent	absent	absent	absent	absent
6	10%	present	present	absent	absent
7	absent	absent	absent	absent	absent
8	absent	absent	absent	absent	absent
10	absent	absent	absent	absent	absent
11	10%	present	present	absent	present
Total*	5	2	2	0	1

Note - * number of tendons which contain changes; absent – changes and cells not visible within specimen

Table 5.5. Changes in muscle in distal portion of specimen

Specimen	% Fibrous and fatty connective tissue	Irregular round shaped myocyte	Myocyte with central nuclei	Inflammatory cells	Heterogenous fibres distribution
1	30%	present	present	absent	present
2	50%	present	present	present	present
3	20-30%	present	present	absent	present
4	50-60%	present	present	present	present
5	30-40%	present	present	absent	present
6	20-30%	present	present	absent	present
7	20-30%	present	present	absent	present
8	20-30%	present	present	absent	present
10	50-60%	present	present	present	present
11	20%	present	present	present	present
Total*	10	10	10	4	10

Note - * number of tendons which contain changes; absent – changes and cells not visible within specimen

5.4. Discussion

The main finding of this study was that there were no arteries found within the tendons of embalmed cadaveric hips using either histological or micro-CT investigation methods.

There were two main aims for this chapter: to investigate the intra-tendinous vascularity of the gluteal tendons; and to compare the accuracy of micro-CT with histology for identifying and quantifying intra-tendinous vessels in the gluteal tendons.

There were no arteries found within the primary, secondary or tertiary bundles or the endotenon of the gluteal tendons. The gluteal tendons are flat tendons and therefore should have intratendinous arteries according to previous studies (Rathbun & MacNab, 1970).

Eight out of the ten specimens were found to have arteries running within the paratenon or epitenon surrounding the tendons suggesting an arterial supply structure described previously for round tendons (Rathbun & MacNab, 1970). This is the first time that the arterial supply structure has been described for the gluteal tendons and we were surprised that they didn't conform to a flat tendon arrangement. However, it is possible that the absence of arteries within the tendon was due to the use of embalmed rather than fresh tissues in this study.

Capillaries were identified within the gluteal tendons adjacent to the enthesis. These were observed in all but two specimens. These vessels were judged to have the appearance of

being secondary to neovascularisation. Neovascularisation is thought to indicate tendon degeneration, which has been shown to occur first, and to be most extensive, in areas of hypovascularity (Lohr & Uthoff, 1990; Fenwick, 2002). In this study, we did not see a clear association between tendon degeneration scores and the presence of neovascularisation. This may indicate that the region around the enthesis is discrete in terms of degeneration because it is subjected to the transmission of force from muscle to bone (Tempfer and Traweger, 2015). Hypoxia has been proposed as an important factor in relation to tendon rupture. It is proposed that hypoxia leads to the histopathological changes of tendon degeneration and subsequent rupture (Fenwick et al., 2002). However, there is no direct evidence proving that hypovascularity is the cause for gluteal tendon rupture; only that within the Achilles and long head of biceps tendons, rupture occurs most frequently within areas of hypovascularity (Fenwick, 2002, Chen et al., 2009; Cheng et al., 2010).

The distance of the neovascularisation to the enthesis varied between abutting the enthesis to 2 mm proximal to the enthesis. In previous studies hypovascularity has been within the distal 20 mm of the Achilles, supraspinatus and infraspinatus tendons (Brooks et al, 1992; Ahmed et al. 2002). It is in this area of hypovascularity that most supraspinatus and infraspinatus tears occurred. In the gluteal tendons, tears also occur in the distal region (Brooks et al. 1992; Howell et al., 2001; Connell et al., 2003; El-Husseiny, 2011) and the neovascularization seen in this region may be an indicator of degenerative changes which may precede a tear.

The tendons used in this study were not documented to be pathological. The Bonar score indicated a degeneration level of between three and eight (out of 15). Maffulli et al. (2008) scored intact and ruptured supraspinatus tendons and reported that intact tendons scored between zero and four; while the ruptured scored between six and twelve. Fearon et al. (2014) undertook a study with fresh gluteal tendons from a cohort of patients undergoing gluteal tendon repair. The highest modified Bonar score described by Fearon et al. (2014) was 14.4 ± 1.5 and reflected areas of worst cell morphology. Therefore, the tendons used in this study were worse than Maffulli's intact supraspinatus tendons but not as severely degenerated as either cohort of ruptured tendons. This indicates that they were degenerated but not torn.

The degenerative changes within the muscle were found to be increased distally. Interestingly, the specimens which had fibrous and fatty connective tissue changes in the proximal portion of the muscles were not the ones with the greatest amount of change in the distal portion of the muscle. Also, the specimens which had the highest modified Bonar score did not have the most degenerative change in the muscle. This finding appears counter-intuitive but may be explained by an imbalance in the degeneration - regeneration cycle within the muscles of these damaged tendons (Gibbons et al, 2017).

Gibbons et al. (2017) have recently postulated a mechanism for muscular degeneration secondary to rotator cuff tears. They describe a cycle of degeneration and repair secondary to unloading the muscle as a result of tendon damage. Unloading of the muscle results in muscle atrophy which causes the extracellular matrix to become stiff, leading to increased

incidence of muscle damage and production of inflammatory cells and factors. Activation and mechanical reloading can lead to regeneration but if tendons respond to this activity by becoming painful the cycle is repeated. In our specimens there was evidence of muscle and tendon degeneration but the severity was not coincidental.

The limitations of this study included the small number of specimens and the use of elderly embalmed cadaveric tissue. That said, the embalming process would not have affected the vascular anatomy or the degree of degeneration. However, embalming may have affected the quality of the histological slides (Wood et al., 2015).

In conclusion, there were no intra-tendinous arteries seen within the gluteal tendons of elderly embalmed cadavers. Therefore, a comparison could not be undertaken between micro-CT angiography and histology as no intra-tendinous arteries were seen with either method. The presence of neovascularisation at the majority of entheses suggests that the gluteal tendons are challenged in older age and degenerative changes are common.

Chapter 6:

Conclusions

Chapter 6: Conclusions.

Gluteus medius and minimus are the primary abductors of the hip joint and stabilise the femoral head in the acetabulum during the stance phase of the gait cycle (Beck et al., 2000; Woyski et al., 2013). Dysfunction of gluteus medius and minimus can lead to an antalgic gait, pain and increased energy cost of ambulation (El-Husseiny et al., 2011). Gluteal tendon tears are a cause of gluteal dysfunction (Williams and Cohen, 2009). Once there is failure of conservative treatment (simple analgesia, physiotherapy, mobilisation aids) there is a paucity of evidence showing long term results for surgical treatments in a condition which can cause a loss of quality of life equal to severe osteoarthritis of the hip joint (Fearon et al., 2014; Ebert et al., 2015).

This thesis was undertaken to examine the arterial supply of the gluteal tendons, and determine whether there are areas of hypovascularity within these tendons. Answering these questions would contribute to a better understanding to the pathophysiology of gluteal tendon tears. Understanding this pathophysiological process is important to surgeons undertaking repair of these tendons. After examination of the embalmed cadaveric gluteal tendons, no arterial vessels were found within any tendons. However, arteries were identified in the surrounding paratenon. This suggests that the gluteal tendons are relatively hypovascular compared to other flat tendons.

Intra-tendinous arterial supply has not previously been investigated using micro-CT. Micro-CT was selected due to its ability to produce high-resolution images of microvascular structures (Zagorchev et al., 2010). However, this technique is limited to ex-vivo specimens of limited size because of radiation exposure, scan time, and the size limitations of the scanner. One of the challenges of developing the methodology for this study was finding a non-toxic contrast media which had a low enough viscosity to penetrate into the microvasculature and a high enough atomic number to create contrast between the vessels and the surrounding soft tissues (Bergeron et al., 2006). Our initial animal study led to the use of barium sulphate suspended in resin. However, this medium may still have been too viscous to penetrate the tiny intra-tendinous vessels. The use of a less viscous contrast media or non-embalmed specimens may have assisted with greater contrast media penetration.

The histological investigation was able to show that there were some vessels within the gluteal tendons. Arterioles were seen to be travelling within the paratenon layer of the gluteal tendon. The second type of vessels that were visualised were capillaries which were assessed to be secondary to neovascularisation and probably represented areas of degenerative tendon at the enthesis. This correlated to the common location of gluteal tendon tears. The use of immunohistochemistry (staining for laminin or CD31) with the histological investigation may have assisted in assessing for arterial vessels within the tendon (Petersen et al., 2002; Marquez et al., 2015).

An interesting finding was the degeneration of muscle more proximal to the tendons. However, this did not seem to correlate to the extent of tendon degeneration. We suggest that this finding is consistent with a paradigm of mechanical unloading followed by muscle remodelling, progressive muscular atrophy and fat accumulation described by Gibbons et al., 2018 in their studies of supraspinatus.

There are a multitude of techniques which have been described for repairing gluteal tendon tears: endoscopic, open trans-osseous, bone suture anchors, and augmented repairs (biologic or synthetic scaffolds) (Ebert et al., 2015). Published endoscopic techniques (totalling 26 patients) have resulted in good outcomes at 12 months, but there were difficulties with being able to access the entire tendon footprint for high-grade gluteal tendon tears (Ebert et al., 2015). Repairs with biological or synthetic scaffolds used to augment a tendon repair have been reported to have early (within procedure) and late (osetolysis and scaffold pullout) failures compared to non-augmented repairs (Chen et al., 2009). The technique with the highest chance of the repair healing would likely be from an open trans-osseous technique including decortication of the greater trochanteric tendon insertions to elicit subchondral bleeding as described by both Walsh et al. (2011) and Davies and Davies (2014).

In terms of surgical intervention and repair, paratenon arterial supply, altered muscle architecture and potential for increased muscle stiffness should be considered. The surgeon needs to consider a procedure that will not strangulate or crush the paratenon, which would likely impair healing due to further compromising the arterial supply of the gluteal tendons.

Tendon repair alone is unlikely to improve the degeneration – regeneration cycle of the proximal musculature, and therefore may not completely resolve the pathology (Gibbons et al., 2018). Rehabilitation of the muscle to optimise its ability to accept load is crucial.

Future studies of fresh tendons from younger specimens are needed to identify whether intra-tendinous arteries are present in non-degenerated gluteal tendons. Further optimisation of the contrast media method, such as a different solvent/resin for the contrast, needs to be undertaken in fresh tissue in order to utilise micro-CT for the investigation of intra-tendinous blood supply. Another avenue of study could be to use Micro-MRI instead of Micro-CT for imaging.

In conclusion, no intra-tendinous arteries were identified in embalmed cadaveric gluteal tendons contrary to previous findings in other flat tendons. This finding supports the hypovascular theory for gluteal tendinopathy and tears but requires verification in young healthy tendons.

References

- Adachi, B. (1928). Das arteriensystem der Japaner. *Anatomie der Japaner*, 1, 364-372.
- Ahmed, I., Lagopoulos, M., McConnell, P., Soames, R., & Sefton, G. (1998). Blood supply of the Achilles tendon. *Journal of orthopaedic research*, 16(5), 591-596.
- Albers, I. S., Zwerver, J., Diercks, R. L., Dekker, J. H., & Van den Akker-Scheek, I. (2016). Incidence and prevalence of lower extremity tendinopathy in a Dutch general practice population: a cross sectional study. *BMC musculoskeletal disorders*, 17(1), 16.
- Anjankar, V. P., Panshewdikar, P. N., Thakre, G., Mane, U., & Tekale, V. (2014). Morphological study on branching pattern of Femoral artery: A Cadaveric study. *Asian Journal of Biomedical and Pharmaceutical Sciences*, 4(28), 34.
- Anwer, D., Karmalkar, A., & Humbarwadi, R. (2013). A study of variations in the profunda femoris artery and its branches. *International Journal of Biomedical and Advance Research*, 4(6), 366-368.
- Beck, M., Sledge, J. B., Gautier, E., Dora, C. F., & Ganz, R. (2000). The anatomy and function of the gluteus minimus muscle. *Bone & Joint Journal*, 82(3), 358-363.
- Benjamin, M., Evans, E., & Copp, L. (1986). The histology of tendon attachments to bone in man. *Journal of anatomy*, 149, 89.
- Benjamin, M., Kumai, T., Milz, S., Boszczyk, B., Boszczyk, A., & Ralphs, J. (2002). The skeletal attachment of tendons—tendon ‘entheses’. *Comparative Biochemistry and Physiology Part A: Molecular & Integrative Physiology*, 133(4), 931-945.

- Bergeron, L., Tang, M., & Morris, S. F. (2006). A review of vascular injection techniques for the study of perforator flaps. *Plastic and reconstructive surgery*, *117*(6), 2050-2057.
- Bilhim, T., Casal, D., Furtado, A., Pais, D., O'Neill, J. E. G., & Pisco, J. M. (2011). Branching patterns of the male internal iliac artery: imaging findings. *Surgical and radiologic anatomy*, *33*(2), 151-159.
- Bird, P., Oakley, S., Shnier, R., & Kirkham, B. (2001). Prospective evaluation of magnetic resonance imaging and physical examination findings in patients with greater trochanteric pain syndrome. *Arthritis & Rheumatology*, *44*(9), 2138-2145.
- Bird, P., Oakley, S., Shnier, R., & Kirkham, B. (2001). Prospective evaluation of magnetic resonance imaging and physical examination findings in patients with greater trochanteric pain syndrome. *Arthritis & Rheumatology*, *44*(9), 2138-2145.
- Bland, J. M., & Altman, D. G. (1999). Measuring agreement in method comparison studies. *Statistical methods in medical research*, *8*(2), 135-160.
- Bradnock, B. (1991). Trochanteric branch of the lateral circumflex femoral artery and its possible role as a vascular pedicle bone graft. *Clinical anatomy*, *4*(3), 223-227.
- Brandtner, C., Hachleitner, J., Buerger, H., & Gaggl, A. (2015). Combination of microvascular medial femoral condyle and iliac crest flap for hemi-midface reconstruction. *International journal of oral and maxillofacial surgery*, *44*(6), 692-696.
- Brooks, C., Revell, W., & Heatley, F. (1992). A quantitative histological study of the vascularity of the rotator cuff tendon. *Bone & Joint Journal*, *74*(1), 151-153.

- Bulla, A., Casoli, C., Farace, F., Mazzarello, V., De Luca, L., Rubino, C., & Montella, A. (2014). A new contrast agent for radiological and dissection studies of the arterial network of anatomic specimens. *Surgical and radiologic anatomy*, 36(1), 79-83.
- Bunker, T., Esler, C., & Leach, W. (1997). Rotator-cuff tear of the hip. *Journal of Bone & Joint Surgery, British Volume*, 79(4), 618-620.
- Chandrasekaran, S., Vemula, S. P., Gui, C., Suarez-Ahedo, C., Lodhia, P., & Domb, B. G. (2015). Clinical features that predict the need for operative intervention in Gluteus medius tears. *Orthopaedic journal of sports medicine*, 3(2), 2-5.
- Chen, J., Xu, J., Wang, A., & Zheng, M. (2009). Scaffolds for tendon and ligament repair: review of the efficacy of commercial products. *Expert review of medical devices*, 6(1), 61-73.
- Chen, S.-h., Chen, M.-m., Xu, D.-c., He, H., Peng, T.-h., Tan, J.-g., & Xiang, Y.-y. (2011). Anatomical study to the vessels of the lower limb by using CT scan and 3D reconstructions of the injected material. *Surgical and radiologic anatomy*, 33(1), 45-51.
- Chen, T. M., Rozen, W. M., Pan, W. r., Ashton, M. W., Richardson, M. D., & Taylor, G. I. (2009). The arterial anatomy of the Achilles tendon: anatomical study and clinical implications. *Clinical anatomy*, 22(3), 377-385.
- Cheng, N. M., Pan, W. R., Vally, F., Le Roux, C. M., & Richardson, M. D. (2010). The arterial supply of the long head of biceps tendon: anatomical study with implications for tendon rupture. *Clinical anatomy*, 23(6), 683-692.

- Chi, A. S., Long, S. S., Zoga, A. C., Read, P. J., Deely, D. M., Parker, L., & Morrison, W. B. (2015). Prevalence and pattern of gluteus medius and minimus tendon pathology and muscle atrophy in older individuals using MRI. *Skeletal radiology*, *44*(12), 1727-1733.
- Choi, S.-W., Park, J.-Y., Hur, M.-S., Park, H.-D., Kang, H.-J., Hu, K.-S., & Kim, H.-J. (2007). An anatomic assessment on perforators of the lateral circumflex femoral artery for anterolateral thigh flap. *Journal of Craniofacial Surgery*, *18*(4), 866-871.
- Chummy, S. S. (2006). Last's Anatomy; Regional and Applied. *English Language Book Society, Churchill Livingstone*, *68*, 75.
- Clarke, S., & Colborn, G. (1993). The medial femoral circumflex artery: its clinical anatomy and nomenclature. *Clinical anatomy*, *6*(2), 94-105.
- Connell, D. A., Bass, C., Sykes, C. J., Young, D., & Edwards, E. (2003). Sonographic evaluation of gluteus medius and minimus tendinopathy. *European radiology*, *13*(6), 1339-1347.
- Davies, J. F., & Davies, D. M. (2014). Surgical technique for the repair of tears to the gluteus medius and minimus tendons of the hip. *JBJS Essential Surgical Techniques*, *4*(2), e11.
- Davies, J. F., Stiehl, J. B., Davies, J. A., & Geiger, P. B. (2013). Surgical treatment of hip abductor tendon tears. *Journal of Bone & Joint Surgery, American Volume*, *95*(15), 1420-1425.

- de Oliveira, L. P., Vieira, C. P., Guerra, F. D. R., de Almeida, M. D. S., & Pimentel, E. R. (2013). Statins induce biochemical changes in the Achilles tendon after chronic treatment. *Toxicology, 311*(3), 162-168.
- Dixit, D., Kubavat, D. M., Rathod, S. P., Patel, M. M., & Singel, T. C. (2011). A study of variations in the origin of profunda femoris artery and its circumflex branches. *International Journal Of Biological and Medical Research, 2*(4), 1084-1089.
- Dixit, D., Mehta, L., & Kothari, M. (2001). Variations in the origin and course of profunda femoris. *Journal of the Anatomical Society of India, 50*(1), 6-7.
- Duparc, F., Thomine, J. M., Dujardin, F., Durand, C., Lukaziewicz, M., Muller, J. M., & Freger, P. (1997). Anatomic basis of the transgluteal approach to the hip-joint by anterior hemimiotomy of the gluteus medius. *Surgical and Radiologic Anatomy, 19*(2), 61-67.
- Ebert, J. R., Bucher, T. A., Ball, S. V., & Janes, G. C. (2015). A review of surgical repair methods and patient outcomes for gluteal tendon tears. *Hip International, 25*(1), 15-23.
- Ebraheim, N., Olexa, T., Xu, R., Georgiadis, G., & Yeasting, R. (1998). The quantitative anatomy of the superior gluteal artery and its location. *American journal of orthopedics (Belle Mead, NJ), 27*(6), 427-431.
- El-Husseiny, M., Patel, S., Rayan, F., & Haddad, F. (2011). Gluteus medius tears: An under-diagnosed pathology. *British Journal of Hospital Medicine, 72*(1), 12-16.

- Fearon, A. M., Cook, J. L., Scarvell, J. M., Neeman, T., Cormick, W., & Smith, P. N. (2014). Greater trochanteric pain syndrome negatively affects work, physical activity and quality of life: a case control study. *The Journal of arthroplasty*, 29(2), 383-386.
- Fenwick, S. A., Hazleman, B. L., & Riley, G. P. (2002). The vasculature and its role in the damaged and healing tendon. *Arthritis Research & Therapy*, 4(4), 252.
- Flack, N., Nicholson, H., & Woodley, S. (2014). The anatomy of the hip abductor muscles. *Clinical anatomy*, 27(2), 241-253.
- Fu, S.-C., Rolf, C., Cheuk, Y.-C., Lui, P. P., & Chan, K.-M. (2010). Deciphering the pathogenesis of tendinopathy: a three-stages process. *BMC Sports Science, Medicine and Rehabilitation*, 2(1), 30.
- Gabrielli, C., Olave, E., Sarmiento, A., Mizusaki, C., & Prates, J. (1997). Abnormal extrapelvic course of the inferior gluteal artery. *Surgical and radiologic anatomy*, 19(3), 139-142.
- Gaida, J. E., Alfredson, L., Kiss, Z. S., Wilson, A. M., Alfredson, H., & Cook, J. L. (2009). Dyslipidemia in Achilles tendinopathy is characteristic of insulin resistance. *Medicine & Science in Sports & Exercise*, 41(6), 1194-1197.
- Gautier, E., Ganz, K., KrÄ¼gel, N., Gill, T., & Ganz, R. (2000). Anatomy of the medial femoral circumflex artery and its surgical implications. *Journal of Bone & Joint Surgery, British Volume*, 82(5), 679-683.
- Gelberman, R. H. (1985). Flexor tendon physiology: tendon nutrition and cellular activity in injury and repair. *Instructional course lectures*, 34, 351-360.

- Ghanavati, S., Lisa, X. Y., Lerch, J. P., & Sled, J. G. (2014). A perfusion procedure for imaging of the mouse cerebral vasculature by X-ray micro-CT. *Journal of neuroscience methods*, 221, 70-77.
- Gibbons, M. C., Singh, A., Anakwenze, O., Cheng, T., Pomerantz, M., Schenk, S., . . . Ward, S. R. (2017). Histological evidence of muscle degeneration in advanced human rotator cuff disease. *Journal of Bone & Joint Surgery, American Volume*, 99(3), 190-199.
- Gibbons, M. C., Singh, A., Engler, A. J., & Ward, S. R. (2018). The role of mechanobiology in progression of rotator cuff muscle atrophy and degeneration. *Journal of orthopaedic research*, 36(2), 546-556.
- Gregor, T., Kochová, P., Eberlová, L., Nedorost, L., Prosecká, E., Liška, V., . . . Zimmermann, P. (2012). Correlating micro-CT imaging with quantitative histology *Injury and skeletal biomechanics* (pp. 173-196): InTech.
- Grimaldi, A., & Fearon, A. (2015). Gluteal tendinopathy: Pathomechanics and implications for assessment and management. *The Journal of Orthopaedic and Sports Physical Therapy*, 45(11), 910-922. doi:10.2519/jospt.2015.5829
- Grob, K., Monahan, R., Gilbey, H., Yap, F., Filgueira, L., & Kuster, M. (2015). Distal extension of the direct anterior approach to the hip poses risk to neurovascular structures: an anatomical study. *Journal of Bone & Joint Surgery, American Volume*, 97(2), 126-132.
- Havaldar, P. P., Myageri, M., & Saheb, S. H. (2014). Study of Medial Circumflex Artery. *International Journal of Anatomy and Research*, 2(2), 380-382.

- Havaladar, P. P., Myageri, M., & Saheb, S. H. (2014). Study of Lateral Circumflex Artery. *International Journal of Anatomy and Research*, 2(2), 397-399.
- Heitmann, C., Kawajah, S., Felmerer, G., & Ingianni, G. (1998). Vascular anatomy of the trochanteric region: a possible donor area for free perforator flaps. *European journal of plastic surgery*, 21(5), 219-221.
- Hoffmann, A., & Pfirrmann, C. (2012). The hip abductors at MR imaging. *European journal of radiology*, 81(12), 3755-3762.
- Howe, W. W., Laceyii, T., & Schwartz, R. P. (1950). A study of the gross anatomy of the arteries supplying the proximal portion of the femur and the acetabulum. *The Journal of Bone & Joint Surgery*, 32(4), 856-866.
- Howell, G., Biggs, R., & Bourne, R. (2001). Prevalence of abductor mechanism tears of the hips in patients with osteoarthritis. *The Journal of arthroplasty*, 16(1), 121-123.
- Kalhor, M., Horowitz, K., Gharehdaghi, J., Beck, M., & Ganz, R. (2012). Anatomic variations in femoral head circulation. *Hip International*, 22(3), 307-312.
- Kasai, T., Suzuki, T., Fukushi, T., Kodama, M., & Chiba, S. (1985). Peripheral distribution of the medial circumflex femoral artery. *Okajimas Folia Anatomica Japonica*, 62(2), 89-97.
- Keen, J. A. (1961). A study of the arterial variations in the limbs, with special reference to symmetry of vascular patterns. *American journal of anatomy*, 108(3), 245-261.
- Khan, K. M., Cook, J. L., Bonar, F., Harcourt, P., & Åstrom, M. (1999). Histopathology of common tendinopathies. *Sports Medicine*, 27(6), 393-408.

- Kingston, M. J., Perriman, D. M., Neeman, T., Smith, P. N., & Webb, A. L. (2016). Contrast agent comparison for three-dimensional micro-CT angiography: A cadaveric study. *Contrast Media & Molecular Imaging, 11*(4), 319-324.
- Koeppen, B. M., & Stanton, B. A. (2017). *Berne and levy physiology e-book*. Elsevier Health Sciences.
- Lachiewicz, P. F. (2011). Abductor tendon tears of the hip: evaluation and management. *Journal of the American Academy of Orthopaedic Surgeons, 19*(7), 385-391.
- Lalović, N., Mališ, M., Korica, M., Cvijanović, R., Simatović, M., & Ilić, M. (2013). Origin of the medial circumflex femoral artery--a cadaver study. *Medicinski Glasnik, 10*(2).
- Lipshutz, B. B. (1916). Studies on the blood vascular tree. I. A composite study of the femoral artery. *The Anatomical Record, 10*(5), 361-370.
- Lohr, J., & Uthoff, H. (1990). The microvascular pattern of the supraspinatus tendon. *Clinical orthopaedics and related research*(254), 35-38.
- Maffulli, N., Longo, U. G., Franceschi, F., Rabitti, C., & Denaro, V. (2008). Movin and Bonar scores assess the same characteristics of tendon histology. *Clinical orthopaedics and related research, 466*(7), 1605-1611.
- Manjappa, T., & Prasanna, L. (2014). Anatomical Variations of the Profunda Femoris Artery and Its Branches—A Cadaveric Study in South Indian Population. *Indian Journal of Surgery, 76*(4), 288-292.

- Márquez, W. H., Gómez-Hoyos, J., Woodcock, S., Arias, L. F., Sampson, T. G., & Gallo, J. A. (2015). The regional microvascular density of the gluteus medius tendon determined by immunohistochemistry with CD31 staining: a cadaveric study. *Hip International*, 25(2), 168-171.
- Millar, N. L., Reilly, J. H., Kerr, S. C., Campbell, A. L., Little, K. J., Leach, W. J., ... & McInnes, I. B. (2012). Hypoxia: a critical regulator of early human tendinopathy. *Annals of the rheumatic diseases*, 71(2), 302-310.
- Nasr, A. Y., Badawoud, M. H., Al-Hayani, A. A., & Hussein, A. M. (2014). Origin of profunda femoris artery and its circumflex femoral branches: anatomical variations and clinical significance. *Folia morphologica*, 73(1), 58-67.
- Orebaugh, S. L. (2006). The femoral nerve and its relationship to the lateral circumflex femoral artery. *Anesthesia & Analgesia*, 102(6), 1859-1862.
- Osti, L., Buda, M., Del Buono, A., Osti, R., Massari, L., & Maffulli, N. (2017). Apoptosis and rotator cuff tears: scientific evidence from basic science to clinical findings. *British medical bulletin*, 122(1), 123-133.
- Pan, W.-R., Cheng, N. M., & Vally, F. (2010). A modified lead oxide cadaveric injection technique for embalmed contrast radiography. *Plastic and reconstructive surgery*, 125(6), 261e-262e.
- Pang, J., Shen, S., Pan, W. R., Jones, I. R., Rozen, W. M., & Taylor, G. I. (2009). The arterial supply of the patellar tendon: anatomical study with clinical implications for knee surgery. *ANZ Journal of Surgery*, 79(s1).

- Pauwels, E., Van Loo, D., Cornillie, P., Brabant, L., & Van Hoorebeke, L. (2013). An exploratory study of contrast agents for soft tissue visualization by means of high resolution X-ray computed tomography imaging. *Journal of microscopy*, 250(1), 21-31.
- Peacock Jr, E. E. (1959). A study of the circulation in normal tendons and healing grafts. *Annals of Surgery*, 149(3), 415.
- Peera, S. A., & Sugavasi, R. (2013). Morphological study of branches of femoral artery in the femoral triangle-a human cadaveric study. *International Journal of Health Sciences and Research*, 3(12), 14-19.
- Petersen, W., Bobka, T., Stein, V., & Tillmann, B. (2000). Blood supply of the peroneal tendons: injection and immunohistochemical studies of cadaver tendons. *Acta Orthopaedica Scandinavica*, 71(2), 168-174.
- Petersen, W., Hohmann, G., Stein, V., & Tillmann, B. (2002). The blood supply of the posterior tibial tendon. *Journal of Bone & Joint Surgery, British Volume*, 84(1), 141-144.
- Pfirschmann, C. W., Chung, C. B., Theumann, N. H., Trudell, D. J., & Resnick, D. (2001). Greater trochanter of the hip: attachment of the abductor mechanism and a complex of three bursae—MR imaging and MR bursography in cadavers and MR imaging in asymptomatic volunteers. *Radiology*, 221(2), 469-477.

- Prakash, Kumari, J., Bhardwaj, A. K., JOSE, B. A., YADAV, S. K., & SINGH, G. (2010). Variations in the origins of the profunda femoris, medial and lateral femoral circumflex arteries: a cadaver study in the Indian population. *Romanian Journal of Morphology and Embryology*, 51(1), 167-170.
- Quinodoz, P., Montandon, D., Pittet, B., Quinodoz, M., & Nussbaum, J.-L. (2002). Barium sulphate and soft-tissue radiology: allying the old and the new for the investigation of animal cutaneous microcirculation. *British journal of plastic surgery*, 55(8), 664-667.
- Ranger, T. A., Wong, A. M., Cook, J. L., & Gaida, J. E. (2015). Is there an association between tendinopathy and diabetes mellitus? A systematic review with meta-analysis. *British Journal of Sports Medicine*, 0, 1-10.
- Rath, S., Hung, L., & Leung, P. (1990). Vascular anatomy of the pronator quadratus muscle-bone flap: a justification for its use with a distally based blood supply. *The Journal of hand surgery*, 15(4), 630-636.
- Rathbun, J. B., & Macnab, I. (1970). The microvascular pattern of the rotator cuff. *Journal of Bone & Joint Surgery, British Volume*, 52(3), 540-553.
- Reddy, S., Ramana, V., & Rao, M. (2007). Absence of inferior gluteal artery: a rare observation. *International Journal of Morphology*, 25(1), 95-98.
- Redmond, J. M., Cregar, W. M., Gupta, A., Hammarstedt, J. E., Martin, T. J., & Domb, B. G. (2015). Trochanteric micropuncture: Treatment for gluteus medius tendinopathy. *Arthroscopy techniques*, 4(1), e87-e90.

- Rees, M., & Taylor, G. I. (1986). A simplified lead oxide cadaver injection technique. *Plastic and reconstructive surgery*, 77(1), 141-145.
- Reid, D. (2016). The management of greater trochanteric pain syndrome: a systematic literature review. *Journal of orthopaedics*, 13(1), 15-28.
- Robertson, W. J., Gardner, M. J., Barker, J. U., Boraiah, S., Lorich, D. G., & Kelly, B. T. (2008). Anatomy and dimensions of the gluteus medius tendon insertion. *Arthroscopy*, 24(2), 130-136.
- Ruegg, M., & Meinen, S. (2014). Histopathology in hematoxylin & eosin stained muscle sections. *Sop no. MDCIA_M*, 1(004).
- Schambach, S. J., Bag, S., Schilling, L., Groden, C., & Brockmann, M. A. (2010). Application of micro-CT in small animal imaging. *Methods*, 50(1), 2-13.
- Schatzker, J., & Brånemark, P.-I. (1969). Intravital observation on the microvascular anatomy and microcirculation of the tendon. *Acta Orthopaedica Scandinavica*, 40(sup126), 1-42.
- Schmidt-Rohlfing, B., Graf, J., Schneider, U., & Niethard, F. U. (1992). The blood supply of the Achilles tendon. *International orthopaedics*, 16(1), 29-31
- Scott, A., Backman, L. J., & Speed, C. (2015). Tendinopathy: update on pathophysiology. *journal of orthopaedic & sports physical therapy*, 45(11), 833-841.
- Senior, H. D. (1924). The description of the larger direct or indirect muscular branches of the human femoral artery: A morphogenetic study. *American Journal of Anatomy*, 33(2), 243-265.

- Sharma, P., & Maffulli, N. (2005). Tendon injury and tendinopathy: healing and repair. *Journal of Bone and Joint Surgery*, 87(1), 187-202.
- Siddharth, P., Smith, N. L., Mason, R. A., & Giron, F. (1985). Variational anatomy of the deep femoral artery. *The Anatomical Record*, 212(2), 206-209.
- Sinkeet, S., Ogeng'o, J., Elbusaidy, H., Olabu, B., & Irungu, M. (2012). Variant origin of the lateral circumflex femoral artery in a black Kenyan population. *Folia morphologica*, 71(1), 15-18.
- Song, W., Bae, S., Han, S., & Koh, K. (2006). Anatomical and radiological study of the superior and inferior gluteal arteries in the gluteus maximus muscle for musculocutaneous flap in Koreans. *Journal of Plastic, Reconstructive & Aesthetic Surgery*, 59(9), 935-941.
- Stecco, C., Macchi, V., Baggio, L., Porzionato, A., Berizzi, A., Aldegheri, R., & De Caro, R. (2013). Anatomical and CT angiographic study of superior gluteal neurovascular pedicle: implications for hip surgery. *Surgical and radiologic anatomy*, 35(2), 107-113.
- Standring, S., Borley, N. R., & Gray, H. (2008). *Gray's anatomy: the anatomical basis of clinical practice*. 40th ed., anniversary ed. [Edinburgh]: Churchill Livingstone/Elsevier
- Suami, H., Taylor, G. I., O'Neill, J., & Pan, W.-R. (2007). Refinements of the radiographic cadaver injection technique for investigating minute lymphatic vessels. *Plastic and reconstructive surgery*, 120(1), 61-67.

- Takano, Y., Kobayashi, H., Yuri, T., Yoshida, S., Naito, A., & Kiyoshige, Y. (2018). Fat infiltration in the gluteus minimus muscle in older adults. *Clinical interventions in aging, 13*, 1011.
- Tansatit, T., Wanidchaphloi, S., & Sanguansit, P. (2008). The anatomy of the lateral circumflex femoral artery in anterolateral thigh flap. *Journal of the Medical Association of Thailand, 91*(9), 1404-1409.
- Tanyeli, E., Üzel, M., Yildirim, M., & Celik, H. (2006). An anatomical study of the origins of the medial circumflex femoral artery in the Turkish population. *Folia morphologica, 65*(3), 209-212.
- Tanyeli, E., Yildirim, M., Üzel, M., & Vural, F. (2006). Deep femoral artery with four variations: a case report. *Surgical and radiologic anatomy, 28*(2), 211-213.
- Tayfur, V., Magden, O., Edizer, M., & Atabey, A. (2010). Anatomy of Vastus Lateralis Muscle Flap. *The Journal of Craniofacial Surgery, 21*(6), 1951-1953.
- Tempfer, H., & Traweger, A. (2015). Tendon vasculature in health and disease. *Frontiers in physiology, 6*, 330.
- Tilley, B. J., Cook, J. L., Docking, S. I., & Gaida, J. E. (2015). Is higher serum cholesterol associated with altered tendon structure or tendon pain? A systematic review. *British Journal of Sports Medicine, 49*(23), 1504-1509. doi:10.1136/bjsports-2015-095100
- Tregaskiss, A. P., Goodwin, A. N., Bright, L. D., Ziegler, C. H., & Acland, R. D. (2007). Three-dimensional CT angiography: A new technique for imaging microvascular anatomy. *Clinical anatomy, 20*(2), 116-123.

- Tsutsumi, M., Nimura, A., & Akita, K. (2019). The Gluteus Medius Tendon and Its Insertion Sites: An Anatomical Study with Possible Implications for Gluteus Medius Tears. *Journal of Bone and Joint Surgery*, *101*(2), 177-184.
- Üzel, M., Tanyeli, E., & Yildirim, M. (2008). An anatomical study of the origins of the lateral circumflex femoral artery in the Turkish population. *Folia morphologica*, *67*(4), 226-230.
- Valdatta, L., Tuinder, S., Buoro, M., Thione, A., Faga, A., & Putz, R. (2002). Lateral circumflex femoral arterial system and perforators of the anterolateral thigh flap: an anatomic study. *Annals of plastic surgery*, *49*(2), 145-150.
- Van Ginckel, A., Thijs, Y., Hesar, N. G. Z., Mahieu, N., De Clercq, D., Roosen, P., & Witvrouw, E. (2009). Intrinsic gait-related risk factors for Achilles tendinopathy in novice runners: a prospective study. *Gait & posture*, *29*(3), 387-391.
- Vazquez, M., Murillo, J., Maranillo, E., Parkin, I., & Sanudo, J. (2007). Patterns of the circumflex femoral arteries revisited. *Clinical anatomy*, *20*(2), 180-185.
- Vegas, M. R., & Martin-Hervas, C. (2013). The superolateral thigh flap: cadaver and computed tomographic angiography studies with a clinical series. *Plastic and reconstructive surgery*, *131*(2), 310-322.
- Walters, J., Solomons, M., & Davies, J. (2001). Gluteus minimus: observations on its insertion. *The Journal of Anatomy*, *198*(2), 239-242.
- Wang, B., Zhao, D., Liu, B., & Wang, W. (2013). Treatment of osteonecrosis of the femoral head by using the greater trochanteric bone flap with double vascular pedicles. *Microsurgery*, *33*(8), 593-599.

- Williams, B. S., & Cohen, S. P. (2009). Greater trochanteric pain syndrome: a review of anatomy, diagnosis and treatment. *Anesthesia & Analgesia*, *108*(5), 1662-1670.
- Windhofer, C., Brenner, E., Moriggl, B., & Papp, C. (2002). Relationship between the descending branch of the inferior gluteal artery and the posterior femoral cutaneous nerve applicable to flap surgery. *Surgical and radiologic anatomy*, *24*(5), 253-257.
- Wong, C. H., & Wei, F. C. (2009). Alternative Vascular Pedicle of the Anterolateral Thigh Flap: The Oblique Branch of the Lateral Circumflex Femoral Artery. *Plastic & Reconstructive Surgery*, *123*(2), 571-577.
- Wood, A., Whiten, S., McVee, J., Issberner, J., Jackson, D., & Herrington, C. S. (2015). Histopathology from the dissecting room: Are cadavers a suitable source of educationally useful histopathology specimens? *Anatomy*, *9*(1).
- Woyski, D., Olinger, A., & Wright, B. (2013). Smaller insertion area and inefficient mechanics of the gluteus medius in females. *Surgical and radiologic anatomy*, *35*(8), 713-719.
- Wu, B., Chen, J., Rosa, T. D., Yu, Q., Wang, A., Xu, J., & Zheng, M. H. (2011). Cellular response and extracellular matrix breakdown in rotator cuff tendon rupture. *Archives of orthopaedic and trauma surgery*, *131*(3), 405-411.
- Xu, D. C., Kong, J. M., & Zhong, S. Z. (1989). The ascending branch of the lateral circumflex femoral artery. A new supply for vascularized iliac transplantation. *Surgical & Radiologic Anatomy*, *11*(4), 263-264.
- Yan, J., Takechi, M., & Hitomi, J. (2013). Variations in the course of the Inferior gluteal nerve and artery: a case report and literature review. *Surgical Science*, *4*(10), 429.

Zagorchev, L., Oses, P., Zhuang, Z. W., Moodie, K., Mulligan-Kehoe, M. J., Simons, M., & Couffinhal, T. (2010). Micro computed tomography for vascular exploration. *Journal of angiogenesis research*, 2(1), 7.

Zlotorowicz, M., Szczodry, M., Czubak, J., & Ciszek, B. (2011). Anatomy of the medial femoral circumflex artery with respect to the vascularity of the femoral head. *Journal of Bone & Joint Surgery, British Volume*, 93(11), 1471-1474.

Appendix 1: Dissection Studies

In order to identify the vessels and their relationships, and also plan the optimal site of contrast injection an exploratory dissection was conducted. This was undertaken on an 86 year old female embalmed cadaveric hemipelvis and lower right limb. The specimen was placed supine on the dissection table.

The femoral triangle was exposed using an initial incision along the length of the inguinal ligament and a second incision from the pubic tubercle to the superomedial aspect of the patella.

The origin of the profunda femoris artery (PFA) was identified at the posterior aspect of the femoral artery. The origin of the lateral circumflex femoral Artery (LCFA) was found to arise from the lateral aspect of the PFA and then coursed over the straight head of the rectus femoris muscle.

The three branches (ascending branch [AB], transverse branch [TB] and descending branch [DB] of the LCFA were observed to arise from a common trunk.

Further dissection was focused on the transverse and ascending branches of the LCFA because these branches were most relevant to the investigation of the lateral hip.

The course of the AB was followed along the borders of rectus femoris and sartorius. It was noted that this vessel gave rise to muscular branches supplying sartorius. Sartorius was transected distal to the muscular branches of the AB. Sartorius was then removed from the ASIS and retracted, keeping the muscular branches intact, and revealing a branch of the AB which passed on the vastus lateralis tendon to the iliac crest.

The TB, having arisen just distal to the AB at their common origin, passed directly to supply the tensor fascia latae muscle.

The origin of the medial circumflex femoral artery (MCFA) was identified at the posteromedial aspect of the PFA. A branch of the MCFA was found to pass between pectineus and the iliopsoas tendon, before the MCFA continued over pectineus, and turned posteriorly and coursed between pectineus and adductor longus.

The specimen was then placed prone to remove the skin and expose gluteus maximus and the posterior thigh muscles. Gluteus maximus was removed from the sacrum and separated from gluteus medius. The branches of the superior gluteal artery were transected along the surface of gluteus maximus thereby preserving their length. Gluteus maximus was removed from the femur to completely expose gluteus medius and reveal the superior gluteal artery (SGA) and inferior gluteal artery (IGA).

A branch of the IGA coursed along the medial aspect of the gluteal medius tendon before diving deep to the tendon.

Posteriorly, the MCFA was observed to pass between quadratus femoris and adductor magnus. The MCFA then traversed over adductor brevis before continuing posteriorly between adductor brevis and adductor longus as what has been described as the descending branch (Kasai et al., 1985). The ascending branch of the MCFA was seen to branch superiorly towards the pubic symphysis.

Attention was then returned to the posterior aspect of the thigh and gluteal region. Arteries arising from branches of the MCFA were observed to cover the posterolateral aspect of the greater trochanter. An artery which originated from the IGA travelled over the gluteus medius tendon and then into the gluteus medius muscle.

The results of this exploratory dissection did not differ from previous anatomical descriptions. Based on the results of this dissection study it was decided that the contrast media injection site would be proximal to the bifurcation of the aorta.